Inorganic Chemistry

pubs.acs.org/IC Article

Computational Evaluation of Potential Molecular Catalysts for Nitrous Oxide Decomposition

Kenneth M. Nicholas,* Chance Lander, and Yihan Shao

Cite This: *Inorg. Chem.* 2022, 61, 14591−14605 Read Online

ACCESS | Metrics & More | Article Recommendations | Supporting Information

ABSTRACT: Nitrous oxide (N_2O) is a potent greenhouse gas (GHG) with limited use as a mild anesthetic and underdeveloped reactivity. Nitrous oxide splitting (decomposition) is critical to its mitigation as a GHG. Although heterogeneous catalysts for N_2O decomposition have been developed, highly efficient, long-lived solid catalysts are still needed, and the details of the catalytic pathways are not well understood. Reported herein is a computational evaluation of three potential molecular (homogeneous) catalysts for N_2O splitting, which could aid in the development of more active and robust catalysts and provide deeper mechanistic insights: one Cu(I)-based, $[(CF_3O)_4Al]Cu$ (**A-1**), and two Ru(III)-based, Cl(POR)Ru (**B-1**) and (NTA)Ru (**C-1**) (POR = porphyrin, NTA = nitrilotriacetate). The structures and energetic viability of potential intermediates and key transition states are evaluated according to a two-stage reaction pathway: (A) deoxygenation (DO), during which a metal−N_2O complex undergoes N−O bond cleavage to produce N_2 and a metal−oxo species and (B) (di)oxygen evolution (OER), in which the metal−oxo species dimerizes to a dimetal−peroxo complex, followed by conversion to a metal−dioxygen species from which dioxygen dissociates. For the (F−L)Cu(I) activator (**A-1**), deoxygenation of N_2O is facilitated by an *O*-bound (F−L)Cu−O−N_2 or better by a bimetallic *N,O*-bonded, (F−L)Cu−NNO−Cu(F−L) complex; the resulting copper−oxyl (F−L)Cu−O is converted exergonically to (F−L)Cu−(η^2,η^2-O_2)−Cu(F−L), which leads to dioxygen species (F−L)Cu(η^2-O_2), that favorably dissociates O_2. Key features of the DO/OER process for (POR)ClRu (**B-1**) include endergonic N_2O coordination, facile N_2 evolution from LR′u−N_2O−RuL to Cl(POR)RuO, moderate barrier coupling of Cl(POR)RuO to peroxo Cl(POR)Ru(O_2)Ru(POR)Cl, and eventual O_2 dissociation from Cl(POR)Ru(η^1-O_2), which is nearly thermoneutral. N_2O decomposition promoted by (NTA)Ru(III) (**C-1**) can proceed with exergonic N_2O coordination, facile N_2 dissociation from (NTA)Ru−ON_2 or (NTA)Ru−N_2O−Ru(NTA) to form (NTA)Ru−O; dimerization of the (NTA)Ru-oxo species is facile to produce (NTA)Ru−O−O−Ru(NTA), and subsequent OE from the peroxo species is moderately endergonic. Considering the overall energetics, (F−L)Cu and Cl(POR)Ru derivatives are deemed the best candidates for promoting facile N_2O decomposition.

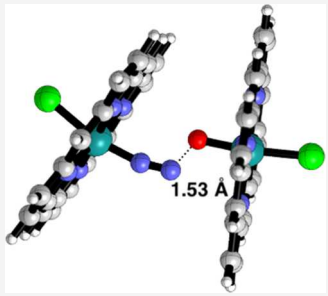

1. INTRODUCTION AND BACKGROUND

Nitrous oxide (N_2O) is an abundant gaseous compound that is thermodynamically unstable relative to its elements, N_2 and O_2 (ΔG_{decomp} −26 kcal/mol), but it is quite unreactive. Its chief use as a mild and nontoxic anesthetic contrasts with its high potency as a greenhouse gas (GHG).[1] The GHG properties of nitrous oxide have stimulated the investigation and technical development of solid catalysts for its mitigation via decomposition[2] (eq 1) or reduction.[3] These reactions have been examined in the context of diesel fuel emissions and methane partial oxidation.[4] Practical limitations of the available heterogeneous (solid) transition metal-supported nitrous oxide decomposition catalysts include their low activity, requiring high operating temperatures, and their ready degradation by common impurities (H_2O, O_2, etc.). Moreover, the details of the catalytic pathways for these systems are not well understood, especially the process leading to oxygen evolution (OE). As for many solid catalysts, the rational design and preparation of improved single-site catalysts remain a considerable challenge.

splitting/decomposition

$$N_2O\text{--(cat)}\rightarrow N_2 + 1/2\ O_2, \qquad \Delta G_{decomp} -26\ \text{kcal/mol} \tag{1}$$

Studies of both reduction and decomposition catalysts, e.g., with Fe- and Cu-zeolites, suggest that N_2O reacts with the reduced metal center (e.g., Cu(I) or Fe(II)) to lose N_2 and to generate a reactive metal−oxide (oxido) species, M−O, which can O−O couple to subsequently produce O_2.[5] On a fundamental level, the association and activation of N_2O by metal zeolites have been probed spectroscopically and computationally. In a study of N_2O−Fe(II) zeolites by IR, Mossbauer, UV−vis spectroscopy, and DFT modeling of N_2O

Received: May 9, 2022
Published: September 6, 2022

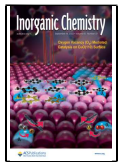

binding by the Sels and Solomon groups monometallic Fe−N binding was formulated at low temperatures, and at higher temperatures, an *O*-bound species and a *bis*-$Fe(N_2O)_2$ species were assigned, which can denitrogenate to Fe═O.[6] These collaborators also computationally modeled a Cu_2 zeolite N_2O-binding site and proposed a bimetallic η^1,η^1-*O*,*O*-Cu-O(N_2)-Cu intermediate at shorter Cu−Cu distance and an monometallic *O*-bound Cu−O−N_2 with a longer Cu−Cu distance.[7]

A deeper knowledge and understanding of metal−N_2O coordination and activation would aid the rational development of more efficient and robust catalysts for N_2O decomposition. More broadly, fundamental experimental and computational reactivity studies of N_2O−transition metal interactions could lead to the discovery and development of new chemical transformations of nitrous oxide, which are presently rather limited.[8] In this vein, gas-phase metal ion−N_2O reactions have been reported and modeled computationally.[9] For the Fe(II)/N_2O system, deoxygenation (DO) to FeO has been observed by MS and modeled in terms of a Fe(II)−O−N_2 intermediate preceding N−O cleavage.[10] Only a few studies of N_2O coordination to well-defined metal complexes in solution have been reported.[11] These feature metal centers in low/mid oxidation states, bonded η^1-*N*-end-on or η^2-side-on (Figure 1).[12−15] A couple of bifunctional,

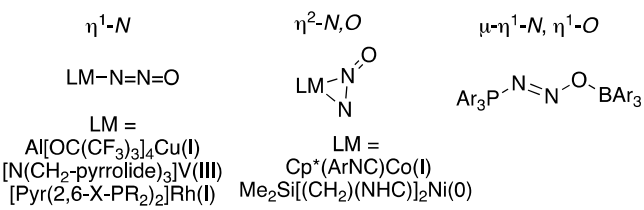

Figure 1. Coordination modes of N_2O established by X-ray diffraction.

N_2O-bridged adducts with frustrated Lewis pairs (FLPs) have also been prepared that show a bent N_2O fragment, suggesting a considerable electronic perturbation of the N_2O unit.[16,17]

Rather little is known of the reactivity of discrete N_2O complexes. Among well-characterized N_2O complexes and presumed adducts, *O*-atom abstraction by a reducing metal center has been observed (eq 2), e.g., by LV(III)[13] and early metallocenes, Cp_2M,[18] breaking a relatively weak N−O bond while forming a strong M−O bond. A rare study of N−O cleavage of various *N*-oxides, including N_2O, by LV(III) to give LV(V)O, showed N_2O to be among the most reactive of O-transfer agents.[13b] Another pathway involving N−O scission of N_2O results in *O*-transfer to an oxidizable substrate, as illustrated by the reaction of N_2O with $RuCl_2L(PPh_3)$,[19] which produces both an oxo−bimetallic species (eq 3) and phosphine oxide. It was also claimed that at low temperature, the Ru−N_2O adduct forms *cis*-$RuCl_2L(PPh_3)(N_2)$ and molecular oxygen, the only example we are aware of in which O_2 is produced from N_2O in a soluble metal complex. Analogously, an FLP−N_2O adduct, when heated, evolves N_2 and the *O*-atom is transferred to a phosphine oxide−BZ_3 product (eq 4).[16] A unique instance of N−N bond cleavage of N_2O comes from its reaction with $Mo[N(R)Ar]_3$ (eq 5).[20]

$$LM + N_2O \rightarrow LMO + N_2 \tag{2}$$

$$RuCl_2L(PPh_3) + N_2O \rightarrow LCl_2Ru{-}O{-}RuLCl_2 + OPPh_3 \tag{3}$$

$$t - Bu_3P{-}N = N{-}O{-}B(C_6F_5)_3 \rightarrow t - Bu_3P{-}O{-}B(C_6F_5)_3 + N_2 \tag{4}$$

$$Mo[N(R)Ar]_3 + N_2O \rightarrow [Ar(R)N]_3Mo(N) + [Ar(R)N]_3Mo(NO) \tag{5}$$

There are a small number of reported N_2O reactions with oxidizable reactants that are catalyzed by soluble, transition metal compounds and which produce N_2 and an oxidized product, e.g., LM-catalyzed oxidation of PPh_3 by N_2O (eq 6),[21] the epoxidation of alkenes (eq 7),[22] and oxidation of alcohols and hydroaromatics (eq 8).[23] The intervening deoxygenation of N_2O by a reduced (TMP)Ru(II) species in the catalysis is supported by the finding that (TMP)Ru(THF) reacts with N_2O at rt to give $(TMP)RuO_{1,2}$.[24] Ruthenium complexes also can catalyze the deoxygenation (reduction) of N_2O by hydrogen[25] or carbon monoxide (eqs 9 and 10).[26] Finally, we note the facile biochemical reduction of N_2O ($N_2O + 2e^- + 2H^+$ --(N_2OR)→ $N_2 + H_2O$) catalyzed by the enzyme nitrous oxide reductase (NOR) at a unique Cu_4S-active site (eq 11).[27] Experimental and computational mechanistic studies on the enzyme and model Cu_xS_y compounds suggest that N_2O is activated by coordination in a bimetallic bridging fashion, followed by reduction and proton transfer.

$$N_2O + PR_3 {-}{-}(LM){\rightarrow} OPR_3 + N_2 \tag{6}$$

$$N_2O + \text{alkene} {-}{-}[(TMP)RuO_2]{\rightarrow} N_2 + \text{epoxide} \tag{7}$$

$$N_2O + \text{alcohol} {-}{-}[(TMP)RuO_2]{\rightarrow} N_2 + \text{ketone} + H_2O \tag{8}$$

$$N_2O + H_2 {-}{-}(LRuH){\rightarrow} N_2 + H_2O \tag{9}$$

$$N_2O + CO {-}{-}(LRuH){\rightarrow} N_2 + CO_2 \tag{10}$$

$$N_2O + 2H^+ + 2e^- {-}{-}(Cu{-}NOR){\rightarrow} N_2 + H_2O \tag{11}$$

There is much still to be learned about the factors that facilitate nitrous oxide activation and its chemical transformation. In the present study, we examine the viable pathways for the transition metal-catalyzed N_2O decomposition to N_2 and O_2. To our knowledge, there are no experimental reports of catalytic N_2O decomposition/splitting by molecular transition metal complexes. The potential for N_2O splitting by Ti(II)(porphyrin) was evaluated computationally, finding that initial N−O cleavage would be facile, but very large activation barriers would exist in steps leading to O_2 evolution.[28] Although homogeneous solution-phase catalysts would not likely be practical for large-scale N_2O decomposition/mitigation, the design and development of such species could 1. provide new insights into the factors controlling the activity and selectivity of the N_2O catalytic decomposition reaction; 2. lead to improved solid catalysts via tethering of designer homogeneous species to solid supports; and 3. identify the structure/reactivity factors that would lead to the development of new catalytic transformations of N_2O. The following are among the important unanswered questions: What qualities of a ligated metal center, LM, influence the affinity for N_2O and its mode of coordination, *N*- vs *O*-, and the favorability of mono- vs bimetallic coordination? How does

https://doi.org/10.1021/acs.inorgchem.2c01598
Inorg. Chem. 2022, 61, 14591−14605

Scheme 1. Two-Stage Reaction Process for Element Oxide, XYO, Splitting Reactions Promoted by an Oxophilic Catalyst LM

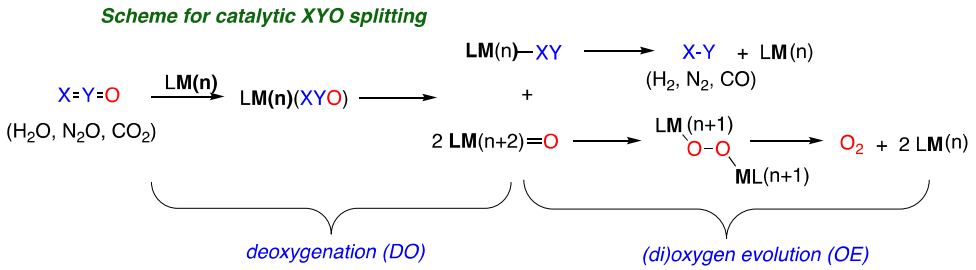

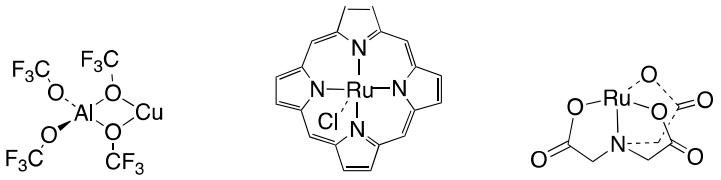

	A-1	B-1	C-1
LM	$[(R_FO)_4Al]Cu(I)$ d^{10}	(POR)ClRu(III) d^5	(NTA)Ru(III) d^5
LMO	$[(R_FO)_4Al]Cu(III)O$ d^8	(POR)ClRu(V)(O) d^3	(NTA)Ru(V)(O) d^3

Figure 2. Catalyst candidates and corresponding oxo-derivatives for nitrous oxide decomposition according to Scheme 1.

the coordination mode affect the energetics of N−O cleavage? What are the energetically viable pathways for the incipient oxo−metal species proceeding to evolve molecular oxygen? We address these questions and others by computationally examining the interaction and subsequent transformations of N_2O with three ligated metal systems, one of copper and two of ruthenium.

1.1. Computational Methods. The B3LYP[29] functional resident in Gaussian 09[30] was used to determine the energy-minimized structures, vibrational frequencies, and electronic energies of stationary point and saddle point species. For the B3LYP optimizations, the 6-31G(d) basis set was used for H, C, N, O, and F atoms, 6-311+G(d,p) for Al, Cl, and S, and LANL2DZ for Cu and Ru. The Gibbs free energies and enthalpies include zero-point vibrational energies and thermal corrections at 298 K. Transition states were approached by single-variable relaxed (mod-redundant) scans and characterized by single imaginary frequencies with displacement along the reaction coordinate and intrinsic reaction coordinate (IRC) scans. Minimum energy crossing points (MECPs) were calculated using the sobMECP program by Lu,[31] which is based on the Harvey MECP search algorithm.[32] Pathways connecting MECPs to reactants and products were generated using Global Reaction Route Mapping (GRRM) 1.22 software.[33] Thermal correction at the MECP was performed using the procedures in the Supporting Information. CYLview[34] was used for visualization of Gaussian output structures. Energies and Cartesian (*x*,*y*,*z*) coordinates for each of the species analyzed are provided in the Supporting Information.

2. RESULTS AND DISCUSSION

2.1. Rationale. We propose a two-stage process for transition metal-mediated nitrous oxide decomposition based on experimental and computational studies of water oxidation and nitrous oxide deoxygenation and decomposition (Scheme 1). The process consists of (A) coordinative deoxygenation (DO) via $LM(N_2O)$ or $LM(N_2O)ML$ to produce a dinitrogen complex $LM-N_2$ (that loses N_2) and an oxo−metal species, LMO, from two-electron oxidation of the LM center and (B) oxygen evolution (OE) via LMO coupling to give a peroxo−metal species, $LM-O_2-ML$, that converts to a metal−dioxygen species, $LM(O_2)$, and subsequently dissociates O_2. This OE pathway has been designated as I2M and has been experimentally and computationally studied in Ru-catalyzed water oxidations.[35,36] The viability of this OER pathway is further supported by the existence of well-characterized metal−peroxo and −dioxygen complexes.[37,38]

2.2. Catalyst Candidates. With consideration to the putative deoxygenation/oxygen evolution of Scheme 1 for N_2O decomposition, we have selected three prospective catalyst systems for reaction modeling based on their unprecedented ability to either coordinate with N_2O (for LCu, **A**) or to produce O_2 (OE) from LMO_x species, LRu(V)O (**B**, **C**) or $L-Cu-O_2$ (**A**). Each of the selected LM species features a low/mid oxidation state metal and is coordinatively unsaturated for favorable N_2O binding. General principles of coordination chemistry structure/reactivity such as oxidation state, total charge, ligand donor/acceptor properties, and coordination number also guided the selection of **A**−**C**. The (fluoroalkoxyaluminate)Cu complex (F−L)Cu (**A-1**) is a computationally simplified, electronically similar model for the experimentally characterized $\{[(CF_3)_3CO]_4Al\}Cu-N_2O$ species that features a weakly coordinating anionic bidentate ligand.[12] We note that the Cu-aluminate unit of **A** is also structurally and electronically similar to the *O*,*O*-silicate/aluminate sites of Cu-zeolites that activate and decompose N_2O.[5−7] We also consider here the N_2O-coordinating ability of other simple Cu(I)X species, including Cu(OTf) (OTf = CF_3SO_3). Less well established is the viability of LCu−O oxyl species that would result from N−O cleavage, though such derivatives have been proposed as biochemical intermediates in enzymatic C−H oxidation.[39] Relevant to the OE reaction is the well-known ability of LCu(I) to reversibly bind/release O_2 via $LCu_{1,2}(O_2)$ in both synthetic and biological systems (Figure 2).[40,41]

We have also selected two LRu(III) systems, (POR)RuCl (**B**) and (NTA)Ru (**C**), for evaluation. Oxide and zeolite-supported Ru catalysts for N_2O decomposition have been

https://doi.org/10.1021/acs.inorgchem.2c01598
Inorg. Chem. 2022, 61, 14591−14605

Scheme 2. B3LYP-Optimized Intermediates and Transition States (TSs) for (F−L)Cu (A-1)-Catalyzed N_2O Splitting[a]

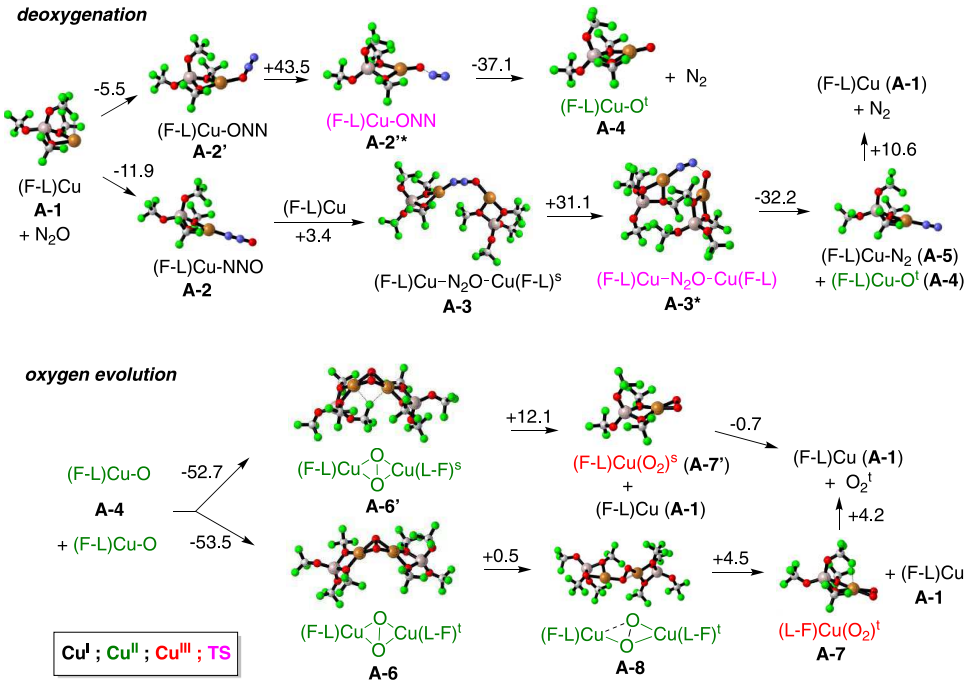

[a]Atomic color key: C = gray, H = white, O = red, N = blue, F = green, Al = silver, and Cu = bronze. Reaction free energies are given over the reaction arrows. Molecular formulae show formal Ru oxidation states by color: Cu(I)—black, Cu(II)—green, and Cu(III)—red; MECP or transition states = magenta text; most stable spin state is given as a superscript (s = singlet, d = doublet, t = triplet).

reported.[42] Key features of these materials include charging at the Ru(III) or Ru(IV) oxidation levels, significant low-temperature activity (<300 °C), instability in the presence of O_2/H_2O, and unknown reaction intermediates. Among molecular species, the more reduced LRu(II) compounds have shown N_2O coordination and activation ability,[19] but there appears to be no precedent for oxygen evolution (OE) from a LRu(IV)O species that would result from N_2O deoxygenation by LRu(II). On the other hand, OE from oxo−Ru(V) species is well established from water oxidation studies,[43] and our recent computational investigation established the viability of (POR)ClRu(V)O and (NTA)Ru(V)O for OE. The (tetraphenylporphyrin)Ru(III)Cl related to **B-1** is reported experimentally,[44] and related oxo−metal species (X)(TTP)Ru(V)O (X = Cl, Ph)[45] have been detected as transient intermediates. The nitrilotriacetate (NTA) complex **C-1** features a common *N*,O_3-tetradentate ligand, but few (NTA)Ru derivatives have been characterized.[46] Since the coordination affinity of N_2O for Ru(III) is unknown, we considered it appropriate to evaluate the potential of LRu(III) species **B-1** and **C-1** to coordinate and deoxygenate N_2O. The differing ligand properties of the **B** and **C** derivatives, i.e., donor atom set, N_4- vs N_3O-, and coordination numbers, 5 vs 4, respectively, allow us to assess the impact of these factors on N_2O coordination and subsequent DO and OE reactions.

2.3. LCu(A-1) + N_2O. The optimized intermediates that were located on the putative deoxygenation−oxygen evolution pathway for (F−L)Cu-catalyzed N_2O splitting are illustrated in Scheme 2 [(F−L) = $(CF_3O)_4Al$]. For the initial association of the unsaturated (F−L)Cu species **A-1** with N_2O, we were able to find stable Cu−N- and Cu−O-bonded N_2O adducts **A-2** and **A-2′**. The binding energy of (F−L)Cu (**A-1**) for N_2O (ΔG_{bind}) is exergonic, −11.9 kcal/mol to form *N*-bound **A-2** and −5.5 kcal/mol to form *O*-bound **A-2′**. The calculated greater stability of the N-coordinated **A-2** (6.7 kcal/mol) is consistent with the experimentally identified $(F_{27}-L)Cu-N_2O$.[12] The *N*-bound complex **A-2** has a linear $Cu-N_2O$ unit (Cu−N−N 177°, N−N−O 180°) and has similar bond lengths to $[(F_{27}-L)_4Al]Cu-N_2O$: $(F_{27}-L)Cu-N_2O$, N−N 1.08 Å, N−O 1.18 Å; calculated for **A-2**: N−N 1.13 Å, N−O 1.18 Å. These are little different from free N_2O (N−N 1.13 Å, N−O 1.18 Å).[47] A more subtle feature in the calculated structure of **A-2** is a short F−Cu contact from the ligand, 2.60 Å, which is also detected in the X-ray structure of $[(F_{27}-L)_4Al]Cu-N_2O$, F−Cu = 2.61 Å. This interaction may stabilize the molecule by increasing the electron count on the coordinatively unsaturated copper atom. The less stable *O*-bonded complex **A-2′** shows a bent $Cu-O-N_2$ unit (124°) and a linear O−N−N fragment (178°). The N−O length of 1.21 Å in the Cu−O−N−N unit is somewhat longer than in N_2O itself (1.18 Å), suggesting some weakening of the N−O bond upon coordination. This notion is also supported by a comparison of the N−N/N−O calculated vibrational stretching frequencies for **A-2** and **A-2′**, which shows *N*-bonded **A-2** to have a higher frequency (2297 cm^{-1}, corr.) than *O*-bonded **A-2′** (2251 cm^{-1}).[48] A generally higher ν(N−N−O) IR absorption for LM−$\underline{N_2}$O vs LM−$\underline{O}-N_2$ is suggested by calculations on the LRu(N_2O) complexes analyzed here as well (vide infra), a feature that could prove useful in the identification of the yet to be discovered *O*-bound complexes.

Analysis of the frontier molecular orbitals (FMOs) (F−L)Cu−N_2O complex **A-2** shows an occupied MO (OMO-3) that is Cu−N π-bonding and N−N and N−O π-antibonding in character (Figure 3). Inspection of the OMOs of *O*-bound **A-2′** reveals that OMO-5 is Cu−O σ-bonding, O−N π-antibonding, and N−N π-bonding. Although no *O*-bound metal−N_2O adducts have been experimentally proven, *O*-coordination and a bent M−O−N geometry have been

https://doi.org/10.1021/acs.inorgchem.2c01598
Inorg. Chem. 2022, 61, 14591−14605

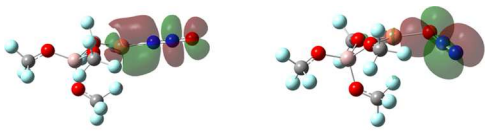

OMO-3 of **A-2** OMO-5 of **A-2'**

Figure 3. Frontier MOs showing Cu−N_2O bonding for (F−L)Cu−N_2O (**A-2**) and (F−L)Cu-ON_2 (**A-2′**); atomic color key: C = gray, N = blue, O = red, F = light blue, Al = pink, and Cu = bronze.

suggested for the gas-phase species Fe^+−N_2O based on DFT calculation.[10c]

To assess the potential ligand electronic effects on the thermodynamic stability of other LCu−N_2O complexes, we calculated the free energy of association of N_2O with various coordinatively unsaturated LCu moieties possessing common anionic ligands (Table 1). Most of these LCu species show

Table 1. Ligand Effects on N_2O Binding Energy to LCu

(L)Cu	ΔG_f (L)Cu−N_2O kcal/mol
$(F_9-L)Cu^a$	−11.9
$(F_{27}-L)Cu^b$	−3.1
$(TfO)Cu^c$	−11.8
$(MsO)Cu^d$	−12.5
(NC)Cu	−12.7
(OAc)Cu	−11.6
(PhS)Cu	−7.9
$(CH_3CN)_3Cu^+$	+4.3

$^a F_9-L = (CF_3O)_4Al^-$. $^b F_{27}-L = [(CF_3)_3CO]_4Al^-$. ^{c}TfO = $CF_3SO_2O^-$. ^{d}MsO = $CH_3SO_2O^-$.

relatively favorable N_2O binding thermodynamics (gas phase, 298 K) in the range of −3 to −12 kcal/mol, except for the positively charged $(CH_3CN)_3Cu^+$ (+4.3 kcal/mol). This behavior is consistent with the presumed weakly basic, π-acceptor ligand properties of N_2O, with binding being favored with more electron-rich (neutral or anionic) LCu fragments. The calculated difference between the F_9− and $(F_{27}-L)Cu$ may result from a combination of the greater steric demand and lesser π-donor ligand electronic effects of the latter complex, which are both destabilizing. It should be noted that in the solid state, most of these LCu species (L = anion) are oligomeric and coordinatively saturated,[49] so stable/detectable N_2O-adducts may only be found in solution with sterically hindered ligands L that ensure a coordination vacancy, such as for the experimental $(F_{27}-L)Cu(N_2O)$.[12]

The most obvious low-energy pathway for N−O cleavage is via the less stable *O*-bound complex, **A-2′**, which would liberate N_2 and form (F−L)Cu−O (**A-4**). The latter was found to be a ground-state triplet ($\Delta G_{trip/sing}$ 33.5 kcal, vide infra, Figure 6), which indicates a spin crossover is needed during the transformation of singlet N_2O complex **A-2′** to oxyl species **A-4**. Searching for a transition state for N−O cleavage, a relaxed coordinate scan along the N−O distance for the singlet of **A-4** failed to show a saddle point; neither did a comparable scan from the higher energy triplet state of **A-2′**. These two scans crossed at an N−O distance of 1.69 Å, providing a starting point to optimize a minimum energy crossing point (MECP) using the sobMECP program.[32] The geometry of the N_2O segment of the MECP structure has a 146° bend, resembling that of the N_2O anion[50] (Figure 4), suggestive of a Cu(II) formulation of the MECP-TS with an electron transfer

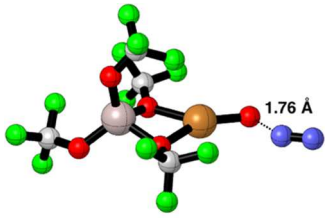

A-2'*

Figure 4. MECP-TS structure for O−N cleavage of (F−L)Cu−O−N_2 (**A-2′***).

to the N_2O unit. From the MECP, an apparent TS was identified, in which the O−N distance was lengthened to 1.76 Å. The electronic activation energy from **A-2′** to MECP/TS **A-2′*** is found to be a substantial 43.4 kcal/mol with a ΔG^* of 43.5 kcal/mol.

A bimetallic intermediate, (F−L)Cu−N_2−O−Cu(F−L) (**A-3**), was also evaluated for its potential to facilitate N−O bond scission. Both a triplet (SI) and a singlet dicopper species were optimized, with the closed shell singlet of **A-3** found to be more stable by 36.0 kcal/mol (Scheme 2). In the singlet species, the N−N−O unit is linear (180°), while the N−O−Cu fragment is distinctly bent (118°), as observed in the monometallic (F−L)Cu−$\underline{N}_2O$ (**A-2**) and (F−L)Cu−$\underline{O}N_2$ (**A-2′**). As in the *O*-bound monometallic **A-2′**, the N−O length of **A-3**, 1.21 Å, is somewhat longer than in free N_2O (N−O 1.18 Å),[48] suggestive of a decreased N−O bond order in both **A-2′** and **A-3**. Inspection of the frontier molecular orbitals (FMOs) of **A-3** found an occupied MO with Cu(1)−N and Cu(2)−O π-bonding and *N,N*- and *N*−*O* π-antibonding character (Figure 5). Although there are as yet no experimentally characterized bimetallic N_2O complexes, we note that the reported FLP adducts $R_3P-N_2O-BR_3$ show more radically distorted N_2O units, e.g., N−N−O (109−111°) and elongated N−O (1.32−1.34 Å) compared to **A-3**.[16,17] DFT modeling of a proposed transient intermediate, (*P,N,P*-L)Rh(I)−N_2O−Rh(I)(*P,N,P*-L), found a ground-state triplet species with a strongly bent M−N_2O−M geometry.[51]

The energetics for singlet bimetallic **A-3** to form (F−L)Cu−O (**A-4**) and (F−L)Cu−N_2 (**A-5**) is nearly thermoneutral (−1.2 kcal/mol), but a spin crossover is required since the Cu−oxyl product **A-4** is calculated to be a ground-state triplet. Mod-redundant scans of the N−O bond distance for the bimetallic singlet and triplet molecules **A-3** indicated a crossing point near 1.5 Å. MECP calculations converged on a structure with an N−O bond length of 1.33 Å (Figure 5). Further scanning of the triplet surface from the MECP located an apparent transition 2.4 kcal/mol higher in energy than the MECP (Figure 5). The TS showed a more elongated N−O distance of 1.57 Å and with major spin density on the Cu(O) unit: $\underline{Cu}$(N) 0.11, $\underline{Cu}$(O) 0.57, $\underline{N}$(Cu) 0.44, $\underline{N}$ 0.03, and $\underline{O}$(Cu) 0.74. The activation energy from the bimetallic singlet **A-3** is 31.1 kcal/mol, considerably lower than that required for N−O cleavage of the monometallic (F−L)Cu−O−N_2 species **A-2′**.

We also considered an alternative bimetallic binding and N−O cleavage mode based on that suggested by Sels and Solomon for N_2O cleavage in the Cu−Cu zeolite site, i.e., an *O,O*-bridged Cu−O(N_2)−Cu species.[7] Unfortunately, we were unable to locate a minimum energy species with this structure derived from **A-1**. However, when the perfluoroalkoxyaluminate ligand was replaced with the *O,O*-bidentate triflate,

https://doi.org/10.1021/acs.inorgchem.2c01598
Inorg. Chem. 2022, 61, 14591−14605

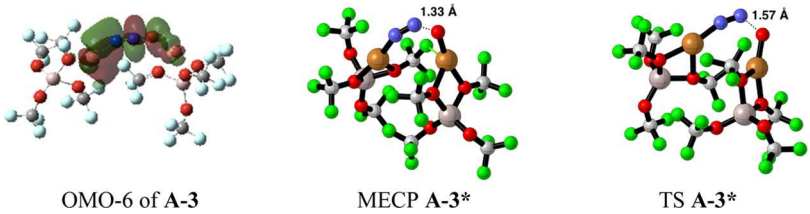

Figure 5. Key FMO of **A-3** and MECP and TS for N−O cleavage **of A-3**.

Scheme 3. Structures and Energetics for (TfO)Cu(η^1,η^1-O−N_2)Cu(OTf) (A′-3) N−O Cleavage via Transition-State A′-3* to Products A′-4 and N_2[a]

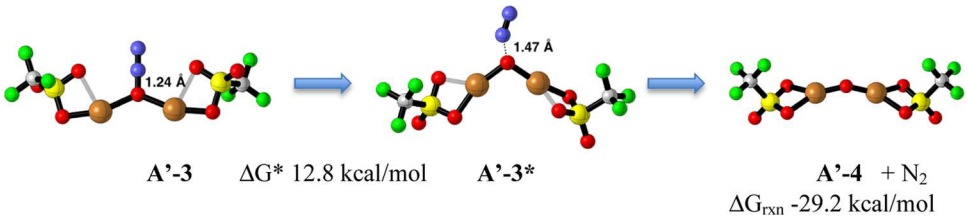

[a]Atomic color key: C = gray, N = blue, O = red, F = green, S = yellow, and Cu = bronze.

($CF_3SO_3^-$), a singlet bimetallic species, (TfO)Cu−(*O*,*O*-N_2O)−Cu(OTf) (**A′-3**), could be optimized, as well as a transition state (**A′-3***) for O−N cleavage (Scheme 3). The activation energy computed for the **A′-3**/**A′-3*** transformation is 12.8 kcal/mol. However, viable access to a peroxo species (TfO)Cu(O_2)Cu(OTf), a requisite for OE via the Cu−oxyl coupling pathway, is doubtful, since the N−O cleavage product (TfO)Cu−O−Cu(OTf) (**A′-4**) failed to form a stable adduct with N_2O, and an alternative intermediate, *bis*-N_2O adduct (TfO)Cu−(O−N_2)$_2$−Cu(OTf), also could not be optimized. Moreover, the energy cost to regenerate (TfO)Cu and (TfO)Cu−O from oxide **A′-4** (25.3 kcal/mol), needed for catalytic turnover, would likely render this a dead-end pathway. Thus, to the extent that triflate is a suitable model for the perfluroroaluminate ligand, it appears unlikely that N_2O deoxygenation via *O*,*O*-bridged **A′-3** and (F−L)Cu−O−Cu(F−L) (**A′-4**) would be the lowest energy pathway for N_2O decomposition.

The oxygen evolution (OE) half-reaction from (F−L)Cu−O oxyl species **A-4** was then evaluated. The majority of the Mulliken electron spin density of **A-4** is localized on the Cu and O-atoms (Cu 0.42 e^-, O 1.51 e^-) and is reflected in the singly occupied MO (SOMO) that is Cu−O π-antibonding (Figure 6). The radical character of **A-4**, with most of its spin density on O and Cu suggests its potential dimerization to a dicopper-peroxide (F−L)Cu(O_2)Cu(F−L). Protein-bound copper−oxyl species analogous to **A-4** have been proposed as reactive intermediates in enzymatic hydroxylation,[40] but experimental or theoretical knowledge of them is quite limited.

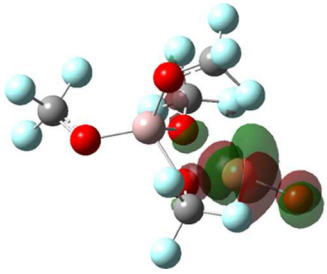

Figure 6. Singly occupied MO (SOMO) for the Cu−oxyl species **A-4**.

The optimized structures of the downstream intermediates derived from Cu−oxyl **A-4** are shown in Scheme 2. The **A-4**/**A-6** oxyl−peroxo conversion is highly exergonic, ΔG −54 kcal/mol. Two peroxo complexes were located and optimized, **A-6** and **A-6′**, both exhibiting a μ,μ-η^2,η^2-bonding mode. The singlet species **A-6′** optimized in an open-shell configuration (antiferromagnetically coupled) with a butterfly-shaped Cu_2O_2 core unit, featuring an O−O distance of 1.41 Å, a Cu−Cu distance of 3.05 Å, and a bridging Cu−F−Cu interaction. The spin densities are located primarily at the Cu atoms (0.41 and −0.44) and less on the bridging O's (0.03, 0.03). The corresponding triplet derivative **A-6** also features a nonplanar, butterfly Cu_2O_2 core with an O−O distance of 1.40 Å and a Cu−Cu length of 3.13 Å. The triplet **A-6** was found to be only 0.8 kcal/mol more stable than the singlet. These peroxo-bridged structures may be compared to that of oxy-hemocyanin, which has an N_3-ligand and a longer Cu−Cu separation of 3.6 Å.[52] Experimental relatives of such μ-peroxo derivatives are well documented in both synthetic[41] and biochemical systems.[42] Our initial efforts to locate a transition state (and activation barrier) for dimerization of the Cu−oxyl **A-4** by various reverse coordinate scans from the peroxo derivatives **A-6**$^{(\prime)}$ were not successful and may be complicated by spin state crossover issues from the transformation of two (F−L)Cu−O triplets (total quintet) to a singlet or triplet peroxo product. The very high exergonicity of this conversion suggests, however, that the barrier would be rather small.

Continuing toward oxygen evolution from the peroxo species **A-6** and **A-6′**, both the triplet and singlet derivatives were investigated for stepwise dissociation of the (F−L)Cu moiety (**A-1**) to form a monometallic dioxygen complex, (F−L)Cu(O_2) (**A-7**$^{(\prime)}$, Scheme 2). In the singlet manifold from **A-6′**, **A-7** was found and optimized as an open-shell singlet species with a symmetrical η^2-coordination mode (Cu−O 2.00, 2.01 Å and O−O 1.28 Å). The majority of electron spin density for this species is centered on the Cu (0.35) and the O−O (−0.21) atoms. Compound **A-7** has spectroscopically identified relatives of similar structure possessing *N*,*N*-bidentate ligands.[53] Transformation of singlet **A-6′** to (F−

https://doi.org/10.1021/acs.inorgchem.2c01598
Inorg. Chem. 2022, 61, 14591−14605

Scheme 4. Free Energy Reaction Profile for (F−L)Cu-Catalyzed N_2O Splitting[a]

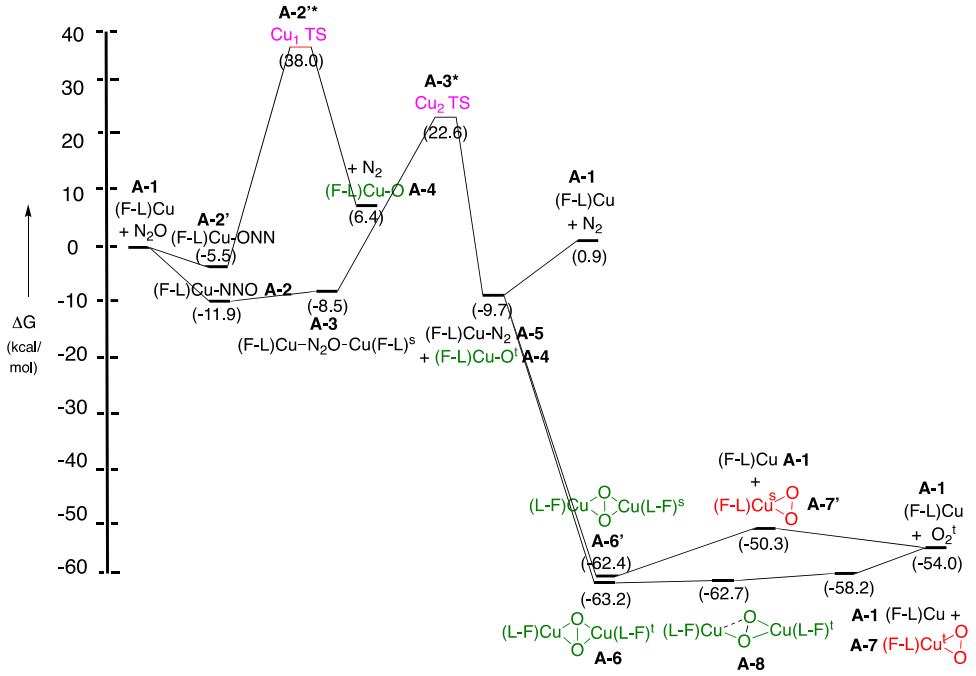

[a](F−L) = $[(CF_3)_3CO]_4Al$; Cu(I) species in black text, Cu(II) species colored green, Cu(III) species in red; spin states, s (singlet), t (triplet), indicated as superscripts; transition states in magenta.

Scheme 5. B3LYP-Optimized Intermediates and Transition States for (POR)ClRu-Catalyzed N_2O Splitting[a]

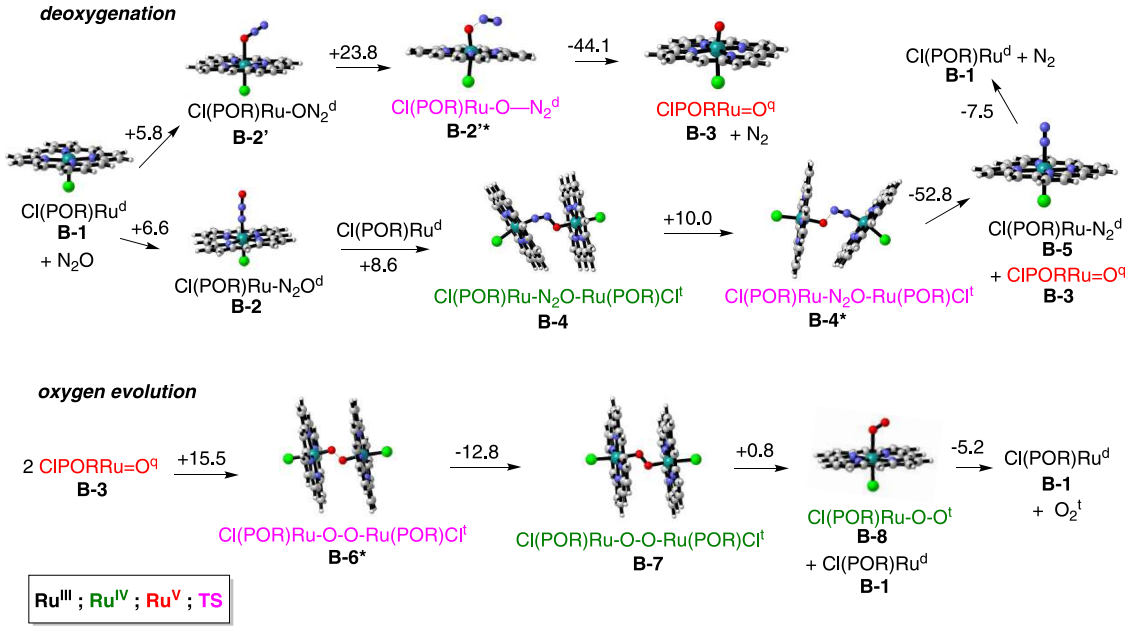

[a]Atomic color key: C = black, H = white, O = red, N = blue, Cl = green, Ru = blue-green. Reaction free energies (kcal/mol) are shown over the reaction arrows. Molecular formulae show formal Ru oxidation states by color: Ru(III)—black, Ru(IV)—green, Ru(V)—red; transition state = magenta text; the most stable spin state is given as superscript, s = singlet, d = doublet, t = triplet.

L)Cu(O_2) (**A-7**) + LCu (**A-1**) is moderately endergonic (+0.1 kcal/mol), with the loss of Cu−O bonding being partially compensated entropically by the formation of two product molecules. Dissociation of triplet dioxygen from the singlet complex **A-7** was calculated to be slightly exergonic at −0.7 kcal/mol. From the more stable triplet peroxo species **A-6**, the oxygen evolution pathway proceeds through a somewhat lower energy set of intermediates. These include an unsymmetrical, semi-bridging peroxo μ-η^1,η^2 species **A-8** that is nearly isoenergetic with the symmetrical peroxo **A-6**. A peroxo complex similar to **A-8** with an unsymmetrical N_3,N_4-ligand has been implicated spectroscopically.[54] Dissociation of (F−L)Cu (**A-1**) from triplet bimetallic **A-6** would produce the triplet η^2-dioxygen complex **A-7**, which is structurally similar to the singlet analogue **A-7′**: Cu−O 2.04 Å, O−O 1.27 Å, but the former is 8.1 kcal/mol more stable. The predominant spin

https://doi.org/10.1021/acs.inorgchem.2c01598
Inorg. Chem. 2022, 61, 14591−14605

density for **A-7** is located on the dioxygen O's (0.85 e^-) and on Cu (0.26 e^-), suggesting that **A-7** may be viewed as a Cu complex of triplet dioxygen. Transition states were not sought for these dissociative transformations along the OE pathway, in part, because the proven facility of the reverse sequence of (F−L)Cu + O_2 reactions to form Cu_2−peroxo species suggests that activation barriers in either direction would not be very high.

The free energy reaction profile for all species evaluated in the (F−L)Cu (**A-1**)-promoted N_2O splitting is provided in Scheme 4. The N−O deoxygenation stage and N−O cleavage step via the dicopper species **A-3**/**A-3*** would likely be turnover-limiting (TL) for N_2O splitting in the lowest energy pathway, while oxygen evolution via the triplet species **A-6**/**A-7**/**A-8** is expected to be relatively facile. These results suggest that (F−L)Cu(I) derivatives are reasonable prospective candidates for moderate-temperature homogeneous catalysis of N_2O decomposition.

2.4. (POR)RuCl (B) + N_2O. The reactants, intermediates, products, and important TSs found for Ru(POR)Cl-promoted N_2O decomposition by the deoxygenation−OER pathway were optimized by the hybrid B3LYP functional. The structures of those species in their ground electronic states are shown in Scheme 5. The oxidation states and electronic spin states are indicated as shown. Note that most monometallic species are found to be ground-state doublets, except for LRuO (quartet) and bimetallic peroxo-triplets, and are indicated accordingly.

Optimized structures were located for an *N*-bound and an *O*-bound N_2O complex, **B-2** and **B-2′**, respectively. The former shows the linear M−N_2O geometry found in the X-ray-determined structures of the reported Cu,V, and Rh complexes.[12−14] Comparing the bond lengths calculated for free N_2O relative to those of **B-2**, the N−N lengths are the same, N−N = 1.13 Å, while the N−O distance is lengthened slightly upon coordination, N−O 1.22 Å in **B-2** vs 1.19 Å in free N_2O, suggesting some weakening of the N−O bond. Comparison of the calculated N−N/N−O vibrational stretching frequencies for **B-2** and **B-2′** shows the *N*-bonded adduct **B-2** to have a higher frequency (2285 cm^{-1}, corr.) than *O*-bonded **B-2′** (2234 cm^{-1}), as observed with the isomeric LCu(N_2O) complexes **A-2**/**A-2′**. The linear geometry is favored by a Ru−N_2O π-(back) bonding interaction most apparent in OMO-12 (Figure 7). The *O*-bound species **B-2′** is

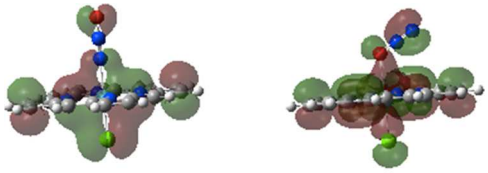

Figure 7. Key bonding interactions for *N*-bound **B-2** and *O*-bound **B-2′** of Cl(POR)Ru(N_2O).

calculated to have a bent M−O−N_2 arrangement (118°) and a linear N_2O moiety (179°). There is little difference in the N−N and N−O bond lengths between **B-2′** and N_2O itself, as shown in parentheses: N−N 1.13 Å (1.13 Å), O−N 1.20 Å (1.19 Å). Although no *O*-bound complexes have been experimentally verified, other *O*-coordinated structures have been proposed with a similarly bent predicted geometry.[50] This arrangement in **B-2′** is favored by a bonding OMO-10 that has a σ-bonding interaction between Ru d_{z^2} and an *O*-p of the π-MO on the N_2O unit. In both **B-2** and **B-2′**, most of the spin density of these doublet species lies on the Ru and Cl atoms and very little on the N_2O unit (e.g., **B-2**: Ru 0.77 e^-, Cl 0.09 e^-, N −0.02 e^-, N 0.008 e^-, O 0.00 e^-; **B-2′**: Ru/POR: Ru 0.81 e^-, Cl 0.08 e^-, N −0.00 e^-, O −0.00 e^-, N 0.00 e^-).

In contrast to the apparent stability of the reported LRu(II)−N_2O species,[19,43] the thermodynamics of N_2O association with the unsaturated Cl(POR)Ru(III) (**B-1**) to form **B-2** and **B-2′** is somewhat unfavorable, +6 (±1 kcal/mol), with *O*-bound **B-2′** slightly more stable (+5.8) than *N*-bound **B-2** (+6.6). The lower affinity of N_2O for LRu(III) relative to LRu(II) is not surprising, given the weakly basic, π-accepting properties of nitrous oxide and the presumably weaker π-donor (back-bonding) ability of Ru(III) relative to Ru(II). However, the inaccuracies of DFT-calculated ligand association/dissociation energies prevent quantitative conclusions.[55] While the limited affinity of Cl(POR)Ru (**B-1**) for N_2O may preclude the isolation of (POR)ClRu(N_2O) (**B-2**/**B-2′**), these species could be accessible in a catalytic system at high concentrations (pressure) of N_2O. Greater N_2O affinity for X(POR)Ru(III) may be achievable through exploitation of the electronic effects of substitution of the axial or porphyrin ligand.[56]

The most obvious low-energy pathway for N−O cleavage is via the *O*-bound complex **B-2′**, from which a strong Ru−O bond can form, yielding (POR)ClRu(V)O (**B-3**) and N_2. A relaxed coordinate scan along the N−O distance helped locate a transition state **B-2′*** (Scheme 5) with an elongated N−O distance (1.47 Å) and a 136° O−N−N angle (Figure 8). A free

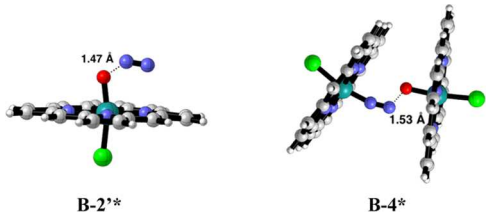

Figure 8. Transition states for N−O cleavage—monometallic **B-2′*** and bimetallic **B-4***.

energy of activation of 25.0 kcal/mol for the transformation **B-2**/**B-2′*** is found. The product (POR)ClRu(V)O (**B-3**) is calculated to be a ground-state quartet under B3LYP (5.7 kcal lower than the doublet). The overall conversion from the N_2O complex to **B-3** and N_2 is thus exergonic by 20.3 kcal/mol. An alternate path for N−O cleavage from the *N*-bound species **B-2** was judged to be highly endergonic, since homolytic N−O cleavage would generate a highly energetic oxygen atom.

We also considered an N−O cleavage pathway that could proceed via a bimetallic intermediate in which N_2O binds in an *N*,*O*-bridging fashion. Both singlet and triplet bimetallic complexes **B-4** were optimized; the triplet **B-4** was found to be more stable than the singlet by 8.0 kcal. The structure of the triplet **B-4** (Scheme 5) features a bent Ru−N_2−O−Ru unit with an N−N−O angle of 122° and an N−O bond length of 1.37 Å, 0.25 Å longer than in the mono-Ru complex **B-2′** and 0.27 longer than in free N_2O. The strongly bent N_2O unit in **B-4** is comparable to that of the bifunctional FLP N_2O-adducts[16,17] and suggests a considerable perturbation of the electronic state of the coordinated N_2O. This notion is supported by a bonding FMO showing Ru−N and Ru−O π-

https://doi.org/10.1021/acs.inorgchem.2c01598
Inorg. Chem. 2022, 61, 14591−14605

bonding, N−N π-antibonding, and N−O σ-bonding character within the Ru−N−N−O−Ru unit (Figure 9). Inspection of the calculated Mulliken atomic charges in the Ru−N_2O−Ru unit supports the idea that there is substantial electron transfer from the (POR)Ru moieties to the N_2O unit (net −0.52 e^- for the *N,N,O*-atoms) vs a net +0.10 e^- in Cl(POR)Ru−ON_2 (**B-2′**). Interestingly, there is also a considerable and unsymmetrically distributed electron spin density on the Ru−N_2O−Ru fragment of **B-4**: Ru(N) 0.23 e^-, N(Ru) −0.11 e^-; N(O) −0.06 e^-; O(Ru) 0.08 e^-, O(Ru) 1.32 e^-. The formation of **B-4** from **B-2** or **B-2′** is thermodynamically uphill, ΔG ca. +9 kcal/mol, and therefore **B-4** would not likely be experimentally detectable by conversion from the monometallic **B-2**.

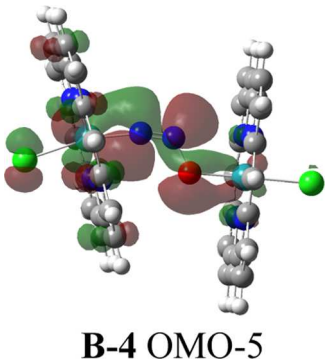

Figure 9. Frontier MO of **B-4** showing bonding interactions in the Ru−N−N−O−Ru moiety.

Completing the deoxygenation stage of the splitting reaction involves N−O bond cleavage of bimetallic **B-4** to Cl(POR)-Ru−O (**B-3**) and Cl(POR)Ru−N_2 (**B-5**). A transition state **B-4*** with triplet character could be located (Figure 8) that features an elongated N−O distance of 1.53 Å (vs 1.37 Å in **B-4**). The activation energy for the **B-4**/**B-4*** cleavage of the N−O bond is a modest 10.0 kcal/mol, considerably lower than the 23.8 kcal for the Cl(POR)Ru−ON_2 **B-2**/**B-2′***, but this is largely counterbalanced by the entropic cost of association to form the bimetallic species. The bimetallic N−O cleavage pathway (**B-1**, **B-2**, **B-4**, **B-4***) is thus modestly favored over the monometallic process (**B-1**, **B-2′**, **B-2′***) based on a lower total activation barrier (25.2 vs 29.6 kcal/mol). The overall conversion from the bimetallic **B-4** to (POR)ClRuO (**B-3**) + Cl(PO)Ru−N_2 (**B-5**) is highly exergonic, −42.8 kcal/mol. The N_2 complex **B-5** (Scheme 5) was found to be a ground-state doublet, with most of the spin density residing on the Ru−Cl unit atom (Ru 0.73 e^-, Cl 0.10 e^-). Complex **B-5** is calculated to release N_2 favorably (ΔG −7.5 kcal/mol), regenerating the reduced Cl(POR)Ru (**B-1**) for further N_2O coordinative activation. The coproduct Ru−oxyl Cl(POR)RuO (**B-3**) was optimized as a ground-state quartet, with the majority of the spin density localized on the Ru (0.93 e^-) and O (0.98 e^-) atoms.

During the oxygen evolution (OE) phase of the N_2O splitting process, Cl(POR)Ru(V)O (**B-3**) is converted via

Scheme 6. B3LYP-Optimized Intermediates and TSs for (NTA)Ru-Catalyzed N_2O Splitting[a]

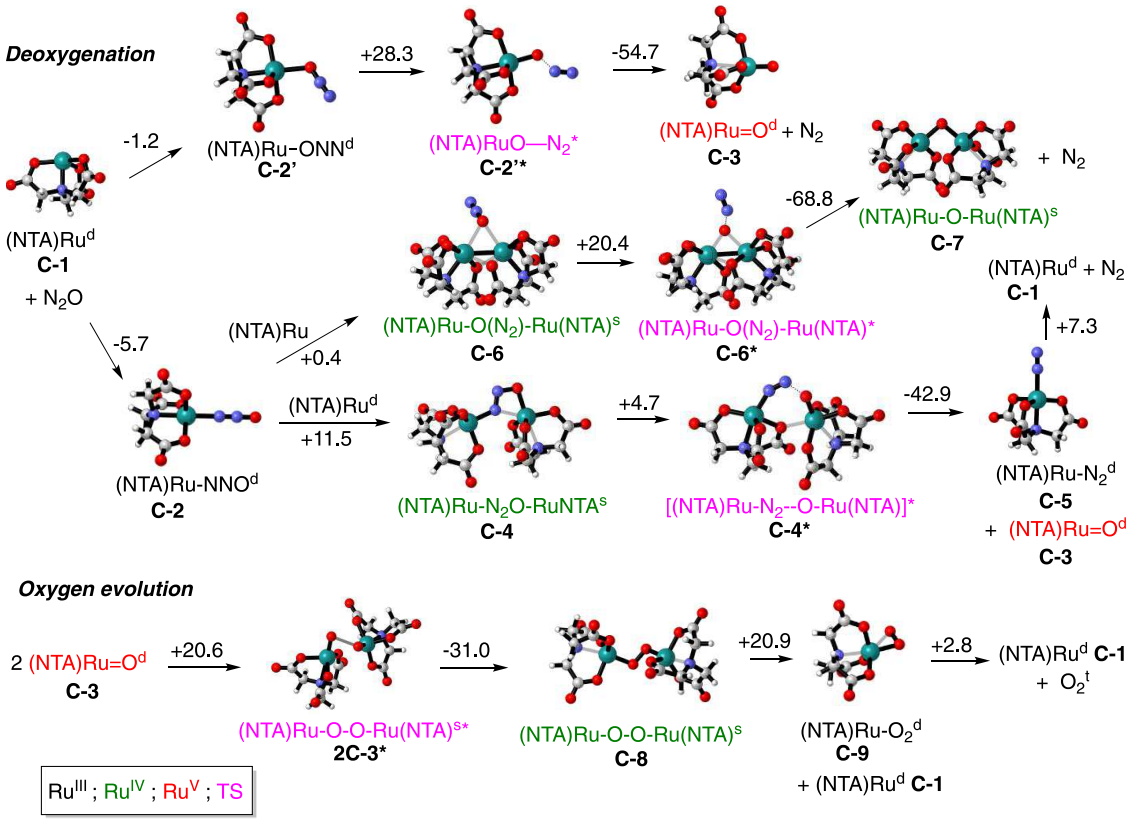

[a]Atomic color key: C = black, H = white, O = red, N = blue, Cl = green, Ru = blue-green; reaction free energies are given over the reaction arrows. Molecular formulae show formal Ru oxidation states: Ru(III)—black, Ru(IV)—green, Ru(V)—red, and transition states—magenta; most stable spin state indicated as superscript, s = singlet, d = doublet, t = triplet.

https://doi.org/10.1021/acs.inorgchem.2c01598
Inorg. Chem. 2022, 61, 14591−14605

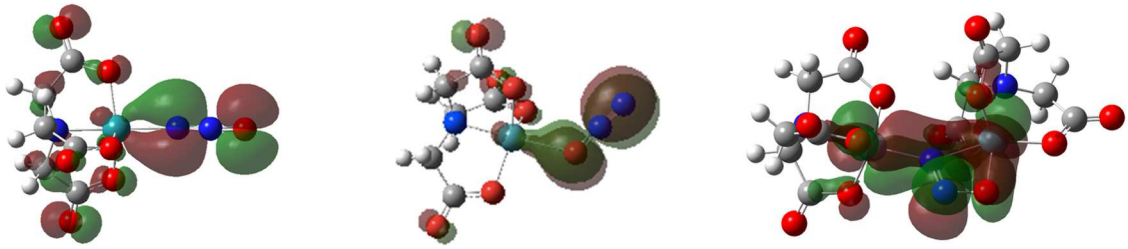

Figure 10. Key occupied molecular orbitals (OMOs) showing bonding character in the Ru−N_2O fragment: OMO-3 of (NTA)Ru−$\underline{N}_2O$ (**C-2**), OMO-4 of (NTA)Ru−$\underline{O}N_2$ (**C-2′**), and OMO-3 of (NTA)Ru−ON_2−Ru(NTA) (**C-4**).

dimerization to a Ru_2 peroxo species, followed by Cl(POR)Ru dissociation to a Ru-dioxygen complex and finally dissociation of the latter to O_2 and Cl(POR)Ru. Since we recently evaluated this sequence computationally in a study of water splitting by various LRu(III) complexes,[57] we will only briefly highlight the key features and energetics here. The intermediates and transition states located for this sequence are summarized in Scheme 5, along with the free energy changes calculated for each step. Key features include the location of a transition state for the O−O coupling of Cl(POR)Ru(O) **B-6*** featuring an O−O distance of 1.71 Å and a modest activation energy of 15 kcal/mol. This leads to the weakly endergonic formation of a μ-η^1,η^1-peroxo derivative **B-7** that is most stable in the triplet state. The peroxo species **B-7** can be transformed via Cl(POR)Ru dissociation to a monometallic dioxygen complex Cl(POR)Ru(η^1-O_2) (**B-8**) with little energy cost; **B-8** is best described as a Ru(IV)-peroxo species. The dissociation of triplet O_2 from **B-8** is calculated to be mildly exergonic. Overall, the thermodynamics of the oxygen evolution half-reaction from the Ru−oxyl **B-3** is almost thermoneutral. Presuming no substantial barriers exist for the nearly thermoneutral dissociation steps, oxygen evolution from Cl(POR)RuO should be a facile thermal process. In support of this notion is the documented reversible dioxygen affinity of some LRu(III) species.[58] For the overall N_2O-decomposition/splitting process with Cl(POR)Ru (**B-1**), N_2O association to give bimetallic **B-4** and its N−O cleavage step (25.2 kcal overall) is calculated to be the turnover-limiting barrier to N_2O decomposition/splitting.

2.5. (NTA)Ru (C-1) + N_2O. The structures of the reactants, intermediates, products, and important transition states resulting from B3LYP optimizations along the (NTA)Ru-N_2O deoxygenation/OER pathway are summarized in Scheme 6. A few generalizations are to be noted initially: the monometallic (NTA)Ru(III)/(V) complexes typically are calculated to have low spin doublet ground states, whereas the bimetallic (NTA)Ru(IV) species are found to be ground-state singlets (e.g., **C-4**, **C-6**, **C-8**). In contrast, recall that the corresponding (POR)RuCl derivatives generally have intermediate spin ground states (Scheme 5).

Association of N_2O with 4-coordinate (NTA)Ru (**C-1**) leads to the *N*-bound and *O*-bound (NTA)Ru(N_2O) complexes, **C-2** and **C-2′**, respectively (Scheme 6). *N*-Coordinated **C-2** shows a nearly linear Ru−N−N−O unit (Ru−N−N angle 177°). As with Cl(POR)Ru−N_2O (**B-2**), the N−N and N−O bond lengths of **C-2**, i.e., 1.13 Å and N−O 1.19 Å, are virtually unchanged from N_2O itself. The structure of the Ru−O species **C-2′** again shows a "bent" Ru−O−N fragment (118°) and N−N and O−O bond lengths, 1.13 and 1.21 Å, little different from free N_2O. Comparison of the calculated N−N/N−O vibrational stretching frequencies for **C-2** and **C-2′** shows the *N*-bonded adduct **C-2** to have a higher frequency (2315 cm^{-1}, corr.) than *O*-bonded **C-2′** (2260 cm^{-1}); the same feature was noted for the *N*- and *O*-bonded (F−L)Cu- and Cl(POR)Ru-(N_2O) pairs, **A-2**/**A-2′** and **B-2**/**B-2′**. The OMO-3 of (NTA)Ru-$\underline{N}_2O$ (**C-2**) shows a Ru-N π-bonding interaction and N−O π-antibonding character (Figure 10). The corresponding (NTA)Ru-$\underline{O}N_2$ OMO-4 features Ru−O d-p π-bonding, O−N π-antibonding, and N−N π-bonding character. In contrast to the Cl(POR)Ru system, complexation of N_2O to the 4-coordinate (NTA)Ru(III) is found to be mildly exergonic, with the *N*-bound species **C-2** somewhat more stable than *O*-bound **C-2′** (ΔG = 4.5 kcal/mol).

A transition state **C-2′*** for N−O cleavage from *O*-bound **C-2′** was located, featuring an elongated O−N distance of 1.76 Å (Scheme 6 and Figure 11). The activation free energy from **C-2′** to **C-2′*** was determined to be 28.3 kcal/mol. Complete cleavage of the N−O bond of **C-2′** results in the release of N_2 and the formation of (NTA)Ru−O (**C-3**); this transformation is highly exergonic (−26.4 kcal/mol). The resulting Ru−oxyl species **C-3** is calculated to be a ground-state doublet, 4.5 kcal/mol more stable than the quartet.

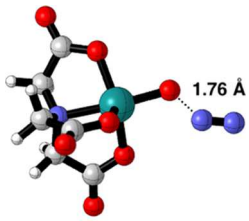

C-2'*

Figure 11. Transition state **C-2′*** for N−O cleavage from monometallic intermediate of **C-2′**.

Association of the monometallic N_2O complexes **C-2** or **C-2′** with another (NTA)Ru species can form an *N*,*O*-bridged complex **C-4**, which could be optimized as either a triplet or singlet species (Scheme 6). The singlet of **C-4** is modestly more stable than the triplet by ca. 4 kcal and features a severely bent N_2O unit (106°) and a novel η^1/η^2-binding mode. This bonding mode is supported by the Ru−d−π-bonding interaction with the N_2O fragment in OMO-3 shown in Figure 10. In comparison with the monometallic complexes, the N−N and N−O bond lengths, 1.25 and 1.34 Å, are considerably longer than for the monometallic **C-2**/**C-2′**. This suggests a substantial perturbation of the electronic character of the N_2O unit, with significant electron transfer from the metal centers, approaching that of the N_2O anion.[52] The triplet (NTA)Ru-N_2O-Ru(NTA) (SI) features a very similar bent/bent structure and bonding mode. Formation of the favored

https://doi.org/10.1021/acs.inorgchem.2c01598
Inorg. Chem. 2022, 61, 14591−14605

bimetallic singlet **C-4** from the mono-Ru N_2O complexes is mildly endergonic (ca. 11 kcal/mol).

Completion of the deoxygenation process via N−O bond cleavage from the bimetallic complex **C-4** could proceed through an optimized transition state **C-4***, as shown in Scheme 6 (Figure 12). In TS **C-4***, the N−O distance is 1.57 Å, 0.23 Å longer than in **C-4**, and the Ru−N−N angle is linearizing. The activation energy for fragmentation of bimetallic **C-4** via **C-4*** was determined to be only 4.7 kcal/mol. An interesting feature of TS **C-4*** is a short Ru−O contact from a bridging NTA carboxylate, which may stabilize the TS relative to the reactant (and products). Completion of the deoxygenation step from **C-4** produces (NTA)Ru-N_2 (**C-5**) and (NTA)Ru-O (**C-3**) in a strongly exergonic step (ΔG = −26.6 kcal). We found both of these species to be favored as ground-state doublets. It is noteworthy that the total activation barrier for N−O cleavage from **C-2** via the bimetallic **C-4** (16.2 kcal) is substantially lower than that from the monometallic **C-2′** (28.3), providing a lower energy pathway for deoxygenation through the bimetallic complex.

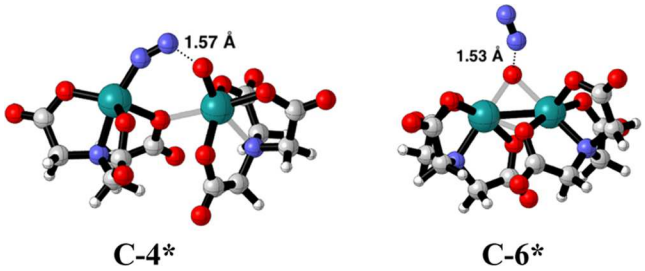

Figure 12. Bimetallic transition states for N−O cleavage of **C-4** and **C-6**.

The alternative bimetallic η^1,η^1-*O,O*-bound species (NTA)-Ru-O(N$_2$)-Ru(NTA) (**C-6**) was also evaluated for its potential intermediacy in the deoxygenation of N_2O (Scheme 6). Dinuclear **C-6** could be optimized to a structure akin to the proposed Cu_2-zeolite derivative[7] with a linear O−N−N unit and O−N of 1.22 Å and N−N of 1.12 Å; the O−N length is modestly longer than found for free N_2O. The *O,O*-bridged species **C-6** is calculated to be 11.1 kcal more stable than the singlet *O,N*-bridged species **C-4**. A transition state **C-6*** for N−O scission from **C-6** was located (N−O length = 1.53 Å) with an activation free energy of 20.4 kcal (Figure 12). Comparing the total activation barriers for N−O cleavage from (NTA)Ru (**C-1**) via the *O,N*-bimetallic species **C-4*** (10.5 kcal/mol) vs *O,O*-bimetallic **C-6*** (15.1 kcal), the pathway via **C-4**/**C-4*** is found to be lower in energy by 4.6 kcal/mol. Thus, although *O,O*-bridged bimetallic **C-6** is calculated to be more stable than **C-4**, the kinetically preferred pathway for OE is likely to proceed via the less stable, *N,O*-bridged species, **C-4**. Additionally, the highly exergonic conversion of *O,O*-bridged **C-6** to the bridged oxide **C-7** may constitute a dead end in catalysis, since Ru(IV) species **C-7** is expected to have little affinity for weakly donating N_2O, and very stable **C-7** will not readily convert to the reactive species (NTA)Ru (**C-1**) and (NTA)Ru−O (**C-3**) (ΔG +39.8 kcal).

The oxygen evolution phases for (NTA)RuO (**C-3**) and six-coordinate L(NTA)RuO (L = Cl, H_2O, NH_3, Pyr) have been described in our recent publication,[59] and so these will only be briefly highlighted here. The species optimized for the OER process are shown in Scheme 6, starting from (NTA)RuO (**C-3**), along with their relative free energies. The dimerization of **C-3** to the ground-state singlet peroxo species (NTA)Ru−O−O−Ru(NTA) (**C-8**) is mildly exergonic (−10.4 kcal), proceeding through a readily located TS **2C-3*** with an activation energy for dimerization of 20.6 kcal. Dissociation of (NTA)Ru (**C-1**) from the peroxo complex **C-8** to produce the η^2-dioxygen complex **C-9** is quite unfavorable (+20.9 kcal). Release of O_2 from **C-9** is also modestly endergonic (+2.8 kcal), completing the OE process. From (NTA)RuO (**C-3**), the overall OE process is substantially endergonic (ca. +20 kcal), while the N−O deoxygenation stage from (NTA)Ru (**1**) and N_2O is substantially exergonic (−32.4 kcal). For this potential catalyst, the overall splitting reaction is anticipated to be kinetically viable at moderate temperatures, with the larger activation (and thermodynamic) barrier coming in the OE phase, i.e., deoxygenation (with N_2 release), is predicted to be easier than O_2 evolution.

We conclude this section with a comparison of the N_2O splitting energetics promoted by (POR)RuCl (**B-1**) and (NTA)Ru (**C-1**) (Scheme 7). The lowest energy intermediates and transition states are shown for each complex. The key comparisons are as follows: (1) the binding energy of N_2O to

Scheme 7. Comparative Lowest Energy Reaction Profiles for N_2O Splitting by Cl(POR)Ru (B-1, in Black) and (NTA)Ru (C-1, in Blue)[a]

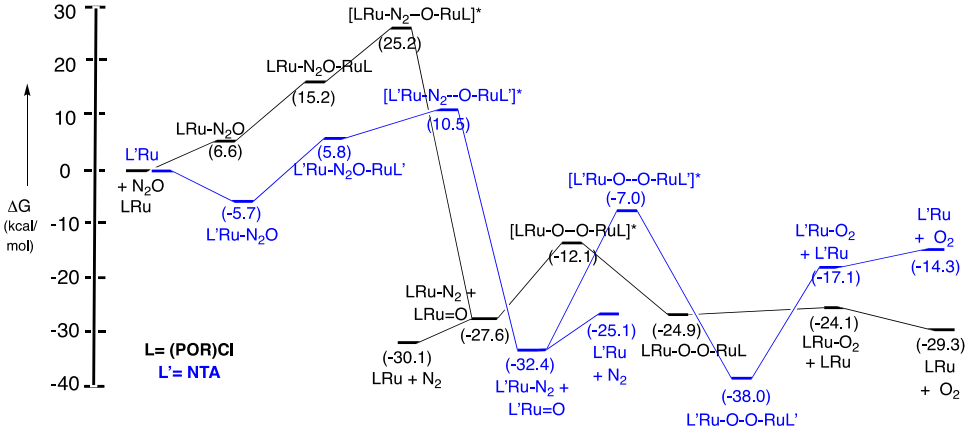

[a]Transition states are indicated by *.

https://doi.org/10.1021/acs.inorgchem.2c01598
Inorg. Chem. 2022, 61, 14591−14605

(NTA)Ru is more favorable than to (POR)RuCl; (2) the activation free energy for N−O scission in monometallic LRu-O-N_2 is similar for both the NTA and POR derivatives (ca. 22−25 kcal); (3) the activation energies for N−O cleavage of the bimetallic complexes are lower relative to the monometallics, i.e., 5−10 vs 22−25 kcal/mol; (4) there is a lower G_{act} for NTA-bimetallic N−O cleavage (5 kcal) than for POR-bimetallic (10 kcal); (5) the oxygen evolution (OE) process for (POR)RuCl is nearly thermoneutral, with a modest O−O coupling barrier (ca. 15 kcal); and (6) the OE for (NTA)Ru is endergonic (ca. +18 kcal) with a larger LRuO coupling activation energy (25 kcal) relative to L = POR (15 kcal). Thus, the deoxygenation/N_2 evolution process should be more facile for (NTA)Ru (**C-1**), while oxygen evolution should be easier for (POR)ClRu (**B-2**). The overall splitting energetics are expected to be similar for the two activators.

Finally, we note that for the (F−L)Cu and Cl(POR)Ru catalysts, N−O deoxygenation (N_2 evolution) is calculated to be turnover-limiting (TL). Comparing the deoxygenation stage for the three catalysts, we found that the activation barriers G_{act} for N−O cleavage via the N_2O-bridged bimetallics to be in the order (NTA)Ru < (F−L)Cu < (POR)ClRu. Key contributors to the activation barrier may be the stability of the preferred bridged bimetallic intermediate, the energetic viability of the incipient metal−oxyl species, and the coordination number. The total activation barriers via bimetallic N_2O-bridged intermediates for these systems (15−25 kcal/mol) suggest that N_2O splitting could be achieved at more moderate temperatures, e.g., <200 °C, than observed for reported solid catalysts. As for the oxygen evolution stage, where the activation barriers are less determined, the thermodynamics of O_2 evolution for these complexes fall in the reverse order (POR)ClRu < (F−L)Cu < (NTA)Ru. The energetics here are dependent on the (in)stability of the intermediate metal−oxyl species and the stability of M−O_2 coordination. For these three representative complexes, the easier the N_2O deoxygenation, the more difficult the O_2 evolution. A significant contributor to the energetic barrier for the turnover-limiting steps is the entropically costly association to form bimetallic complexes with N_2O and for O_2 generation. It may thus be possible to further lower the energy requirements for N_2O decomposition by developing catalysts that have binucleating ligands that preorganize the metal centers, e.g., cofacial porphyrins.[59] Next-generation catalyst candidates incorporating this design element are under consideration.

3. CONCLUSIONS

The energetic and mechanistic viability of nitrous oxide decomposition (splitting) catalyzed by three molecular complexes, (F−L)Cu (**A-1**), Cl(POR)Ru (**B-1**), and (NTA)Ru (**C-1**), have been evaluated in a two-stage reaction pathway involving initial deoxygenation (with N_2 evolution) and (di)oxygen evolution via metal−oxo coupling. (F−L)Cu (**A-1**) is determined to be capable of deoxygenating N_2O to release N_2 with a low barrier via an *O*-bound monometallic or, more readily, by a bimetallic N_2O-bridged complex. Oxygen evolution from LCu−O (**A-4**) is thermodynamically favorable and unlikely to have significant kinetic barriers, rendering overall N_2O splitting by (F−L)Cu species to be kinetically viable at moderate temperatures. There are significant ligand effects on the energetics of the DO and OE for N_2O decomposition by Cl(POR)Ru (**B-1**) and (NTA)Ru (**C-1**). Although N_2O binding to five-coordinate Cl(POR)Ru(III) is relatively unfavorable, subsequent deoxygenation via an *O*-bound monometallic or better *N*,*O*-bridged bimetallic derivatives is more favorable, with moderate activation barriers. The OE process from Cl(POR)RuO is calculated to be both thermodynamically and kinetically favorable, leading to the prediction that N_2O decomposition catalyzed by Cl(POR)Ru will be probable at moderate temperatures. In contrast, N_2O deoxygenation with N_2 generation is relatively more favorable by the four-coordinate (NTA)Ru species, particularly via the *N*,*O*-bridged bimetallic intermediate. On the other hand, oxygen evolution from (NTA)RuO is more energetically challenging because of the expectedly greater stability of the intermediate $(NTA)_2Ru_2$ peroxo species. Finally, we hope that this investigation will stimulate experimental studies, leading to improved systems for nitrous oxide splitting and to other N_2O conversion processes.

■ ASSOCIATED CONTENT

Supporting Information

The Supporting Information is available free of charge at https://pubs.acs.org/doi/10.1021/acs.inorgchem.2c01598.

xyz coordinates for all optimized structures (XYZ)

Calculated energies for optimized structures, MECPs, and MECP free energy corrections (PDF)

■ AUTHOR INFORMATION

Corresponding Author

Kenneth M. Nicholas − *Department of Chemistry and Biochemistry, Stephenson Life Sciences Research Center, University of Oklahoma, Norman, Oklahoma 73019, United States;* orcid.org/0000-0002-5180-1671; Email: knicholas@ou.edu

Authors

Chance Lander − *Department of Chemistry and Biochemistry, Stephenson Life Sciences Research Center, University of Oklahoma, Norman, Oklahoma 73019, United States*

Yihan Shao − *Department of Chemistry and Biochemistry, Stephenson Life Sciences Research Center, University of Oklahoma, Norman, Oklahoma 73019, United States;* orcid.org/0000-0001-9337-341X

Complete contact information is available at: https://pubs.acs.org/10.1021/acs.inorgchem.2c01598

Notes

The authors declare no competing financial interest.

■ ACKNOWLEDGMENTS

The authors are grateful for the financial support provided by the NSF (CHE 1566213 to K.M.N.; CHE 2102071 to Y.S.), a Cope Scholar Award (K.M.N.), and for computing services of the Oklahoma Supercomputer Center for Education and Research (OSCER). The authors also acknowledge helpful discussions with OU colleagues Dr. George Richter-Addo and Matthew Swann.

■ REFERENCES

(1) Singh, S. N.; Tyagi, L. Nitrous Oxide: Sources, Sinks and Mitigation Strategies. In *Nitrous Oxide Emissions Research Progress*; Sheldon, A. I.; Barnhart, E. P., Eds.; Nova Science Publishers Inc., 2009; pp 127−150.

(2) (a) Jabłońska, M.; Palkovits, R. It is no laughing matter: nitrous oxide formation in diesel engines and advances in its abatement over rhodium-based catalysts. *Catal. Sci. Technol.* **2016**, *6*, 7671−7687. (b) Konsolakis, M. Recent Advances on Nitrous Oxide (N_2O) Decomposition over Non-Noble-Metal Oxide Catalysts: Catalytic Performance, Mechanistic Considerations, and Surface Chemistry Aspects. *ACS Catal.* **2015**, *5*, 6397−6421. (c) Shoonheydt, R. A.; Vanelderen, P.; Sels, B. F. Direct catalytic decomposition of N2O over Cu- and Fe-zeolites. In *New and Future Developments in Catalysis: Catalysis for Remediation and Environmental Concerns*; Suib, S. L., Ed.; Elsevier, 2013; pp 399−419.

(3) (a) Jacobs, L.; Barroo, C.; Gilis, N.; Lambeets, S. V.; Genty, E.; Visart de Bocarme, T. Structure reactivity relationships during N_2O hydrogenation over Au-Ag alloys: A study by field emission techniques. *Appl. Surf. Sci.* **2018**, *435*, 914−919. (b) Shi, N.-G.; Zhang, J.-H.; Wang, Y.-C. On the gas-phase PtO^{n+} (n = 1, 2) catalyzed reduction of N_2O by H_2: A density functional study. *Comput. Theor. Chem.* **2013**, 78−84. (c) Arenas-Alatorre, J.; Gomez-Cortes, A.; Avalos-Borja, M.; Diaz, G. Surface Properties of Ni-Pt/SiO_2 Catalysts for N_2O Decomposition and Reduction by H_2. *J. Phys. Chem. B* **2005**, *109*, 2371−2376.

(4) (a) Chmielarz, L.; Kustrowski, P.; Kruszec, M.; Dziembaj, R.; Cool, P.; Vansant, E. F. Nitrous Oxide Reduction with Ammonia and Methane Over Mesoporous Silica Materials Modified with Transition Metal Oxides. *J. Porous Mater.* **2005**, *12*, 183−191. (b) Aika, K.-I.; Oshihara, K. Nitrous oxide reduction with ammonia over Co-MgO catalyst and the influence of excess oxygen. *Catal. Today* **1996**, *29*, 123−126. (c) Rondinelli, F.; Russo, N.; Toscano, M. On the Pt^+ and Rh^+, Catalytic Activity in the Nitrous Oxide Reduction by Carbon Monoxide. *J. Chem. Theory and Comput.* **2008**, *4*, 1886−1890. (d) Rondinelli, F.; Russo, N.; Toscano, M. On the origin of the different performance of iron and manganese monocations in catalyzing the nitrous oxide reduction by carbon oxide. *Inorg. Chem.* **2007**, *46*, 7489−7493. (e) A commercial Cu−ZnO N_2O decomposition catalyst : https://catalysts.basf.com/files/pdf/BF-9834_US_N2O_and_DeNOX_Technote.pdf.

(5) Lin, F.; Andana, T.; Wu, Y.; Szanyi, J.; Wang, Y.; Gao, F. Catalytic site requirements for N_2O decomposition on Cu-, Co-, and Fe-SSZ-13 zeolites. *J. Catal.* **2021**, *401*, 70−80.

(6) (a) Bols, M. L.; Snyder, B. E. R.; Rhoda, H. M.; Cnudde, H. M.; Cnudde, P.; Fayad, G.; Fayad, G.; Schoonheydt, R. A.; Schoonheydt, R. A.; Van Speybroeck, V.; Van Speybroeck, V.; Solomon, E. I.; Solomon, E. I.; Sels, B. F. Coordination and activation of nitrous oxide by iron zeolites. *Nat. Catal.* **2021**, *4*, 332−340. (b) Snyder, B. E. R.; Bols, M. L.; Schoonheydt, R. A.; Sels, B. F.; Solomon, E. I. Iron and Copper Active Sites in Zeolites and Their Correlation to Metalloenzymes. *Chem. Rev.* **2018**, *118*, 2718−2768. (c) Sklenak, S.; Andrikopoulos, P. C.; Boekfa, B.; Jansang, B.; Nováková, J.; Benco, L.; Bucko, T.; Hafner, J.; Dedecek, J.; Sobalík, Z. N_2O decomposition over Fe-zeolites: Structure of the active sites and the origin of the distinct reactivity of Fe-ferrierite, Fe-ZSM-5, and Fe-beta. A combined periodic DFT and multispectral study. *J. Catal.* **2010**, *272*, 262−274.

(7) Tsai, M.-L.; Hadt, R. G.; Vanelderen, P.; Sels, B. F.; Schoonheydt, R. A.; Solomon, E. I. $[Cu_2O]^{2+}$ Active Site Formation in Cu−ZSM-5: Geometric and Electronic Structure Requirements for N_2O Activation. *J. Am. Chem. Soc.* **2014**, *136*, 3522−3529.

(8) Severin, K. Synthetic Chemistry with Nitrous Oxide. *Chem. Soc. Rev.* **2015**, *44*, 6375−6386.

(9) Lavrov, V. V.; Blagojevic, V.; Koyanagi, G.; Orlova, G.; Bohme, D. Gas-Phase Oxidation and Nitration of First-, Second-, and Third-Row Atomic Cations in Reactions with Nitrous Oxide: Periodicities in Reactivity. *J. Phys. Chem A* **2004**, *108*, 5610−5624.

(10) (a) Blagojevic, V.; Orlova, G.; Bohme, D. K. O-Atom Transport Catalysis by Atomic Cations in the Gas Phase: Reduction of N_2O by CO. *J. Am. Chem. Soc.* **2005**, *127*, 3545−3555. (b) Rondinelli, F.; Russo, N.; Toscano, M. On the origin of the different performance of iron and manganese monocations in catalyzing the nitrous oxide reduction by carbon oxide. *Inorg. Chem.* **2007**, *46*, 7489−7493. (c) Zhao, L.; Wang, Y.; Guo, W.; Shan, H.; Lu, X.; Yang, T. Theoretical Investigation of the Fe^+-Catalyzed Oxidation of Acetylene by N_2O. *J. Phys. Chem. A* **2008**, *112*, 5676−5683.

(11) Tolman, W. B. Binding and Activation of N_2O at Transition-Metal Centers: Recent Mechanistic Insights. *Angew. Chem., Int. Ed.* **2010**, *49*, 1018−1024.

(12) Zhuravlev, V.; Malinowski, P. J. A Stable Crystalline Copper(I)−N_2O Complex Stabilized as the Salt of a Weakly Coordinating Anion. *Angew. Chem., Int. Ed.* **2018**, *57*, 11697−11700.

(13) (a) Piro, N. A.; Lichterman, M. F.; Harman, W. H.; Chang, C. J. A Structurally Characterized Nitrous Oxide Complex of Vanadium. *J. Am. Chem. Soc.* **2011**, *133*, 2108−2111. (b) Palluccio, T. D.; Rybak-Akimova, E. V.; Majumdar, S.; Cai, X.; Chui, M.; Temprado, M.; Silvia, J. S.; Cozzolino, A. F.; Tofan, D.; Velian, A.; Cummins, C. C.; Captain, B.; Hoff, C. D. Thermodynamic and Kinetic Study of Cleavage of the N-O Bond of *N*-Oxides by a Vanadium(III) Complex: Enhanced Oxygen Atom Transfer Reaction Rates for Adducts of Nitrous Oxide and Mesityl Nitrile Oxide. *J. Am. Chem. Soc.* **2013**, *135*, 11357−11372.

(14) Gyton, M. R.; Leforestier, B.; Chaplin, A. B. Rhodium(I) Pincer Complexes of Nitrous Oxide. *Angew. Chem., Int. Ed.* **2019**, *58*, 15295−15298.

(15) (a) Mokhtarzadeh, C. C.; Chan, C.; Moore, C. E.; Rheingold, A. L.; Figueroa, J. S. Side-On Coordination of Nitrous Oxide to a Mononuclear Cobalt Center. *J. Am. Chem. Soc.* **2019**, *141*, 15003−15007. (b) Puerta Lombardi, B. M.; Gendy, C.; Gelfand, B. S.; Bernard, G. M.; Wasylishen, R. E.; Tuononen, H. M.; Roesler, R. Side-on Coordination in Isostructural Nitrous Oxide and Carbon Dioxide Complexes of Nickel. *Angew. Chem., Int. Ed.* **2021**, *60*, 7077−7081.

(16) Otten, E.; Neu, R. C.; Stephan, D. W. Complexation of Nitrous Oxide by Frustrated Lewis Pairs. *J. Am. Chem. Soc.* **2009**, *131*, 9918−9919.

(17) Mo, Z.; Kolychev, E. L.; Rit, A.; Campos, J.; Niu, H.; Aldridge, S. Facile Reversibility by Design: Tuning Small Molecule Capture and Activation by Single Component Frustrated Lewis Pairs. *J. Am. Chem. Soc.* **2015**, *137*, 12227−12230.

(18) (a) Bottomley, F.; Lin, I. J. B.; Mukaida, M. Reactions of dinitrogen oxide (nitrous oxide) with dicyclopentadienyltitanium complexes including a reaction in which carbon monoxide is oxidized. *J. Am. Chem. Soc.* **1980**, *102*, 5238. (b) Walter, M. D.; Sofield, C. D.; Andersen, R. A. Preparation and Reactions of Base-Free Bis(1,3-di-*tert*-butylcyclopentadienyl)titanium, Cp'_2Ti, and Related Compounds. *Organometallics* **2008**, *27*, 2959.

(19) Pamplin, C. B.; Ma, E. S. F.; Safari, N.; Rettig, S. J.; James, B. R. The Nitrous Oxide Complex, $RuCl_2(\eta^1\text{-}N_2O)(P\text{-}N)(PPh_3)$ (P-N = [o-(N,N-Dimethylamino)phenyl]- diphenylphosphine); Low Temperature Conversion of N_2O to N_2 and O_2. *J. Am. Chem. Soc.* **2001**, *123*, 8596−8597.

(20) (a) Cherry, J. P. F.; Johnson, A. R.; Baraldo, L. M.; Tsai, Y.-C.; Cummins, C. C.; Kryatov, S. V.; Kryatov, S. V.; Rybak-Akimova, E. V.; Rybak-Akimova, E. V.; Capps, K. B.; Capps, K. B.; Hoff, C. D.; Hoff, C. D.; Haar, C. M.; Haar, C. M.; Nolan, S. P. On the Origin of Selective Nitrous Oxide N-N Bond Cleavage by Three-Coordinate Molybdenum(III) Complexes. *J. Am. Chem. Soc.* **2001**, *123*, 7271−7286. (b) Cavigliasso, G.; Criddle, A.; Kim, H.-S.; Stranger, R.; Yates, B. F. On the selective cleavage of nitrous oxide by metal−amide complexes. *Dalton Trans.* **2014**, *43*, 4631.

(21) (a) Yamamoto, A.; Kitazume, S.; Pu, L. S.; Ikeda, S. Synthesis and properties of hydridodinitrogentris(triphenylphosphine) cobalt-(I) and the related phosphine-cobalt complexes. *J. Am. Chem. Soc.* **1971**, *93*, 371. (b) Chernysheva, A. N.; Beloglazkina, E. K.; Moiseeva, A. A.; Antipin, R. L.; Zyk, N. V.; Zefirov, N. S. Co(II) complex of N-[2-(phenylseleno)cyclohexyl]-N-(pyridin-2-ylmethylene) amine: Synthesis, electrochemistry and catalysis of triphenylphosphine and norbornene oxidation by nitrous oxide. *Mendeleev Commun.* **2012**, *22*, 70. (c) Yamada, T.; Suzuki, K.; Hashimoto, K.; Ikeno, T. N_2O oxidation of phosphines catalyzed by low-valent nickel complexes. *Chem. Lett.* **1999**, *28*, 1043.

(22) Yamada, T.; Hashimoto, K.; Kitaichi, Y.; Suzuki, K.; Ikeno, T. Nitrous Oxide Oxidation of Olefins Catalyzed by Ruthenium Porphyrin Complexes. *Chem. Lett.* **2001**, *30*, 268−269.
(23) Hashimoto, K.; Tanaka, H.; Ikeno, T.; Yamada, T. Selective Nitrous Oxide Oxidation for C-H Oxidation and Aromatization of 9,10-Dihydroanthracene Derivatives. *Chem. Lett.* **2002**, *31*, 582−583.
(24) Groves, J. T.; Roman, J. S. Nitrous Oxide Activation by a Ruthenium Porphyrin. *J. Am. Chem. Soc.* **1995**, *117*, 5594−5595.
(25) (a) Zeng, R.; Feller, M.; Ben-David, Y.; Milstein, D. Hydrogenation and Hydrosilylation of Nitrous Oxide Homogeneously Catalyzed by a Metal Complex. *J. Am. Chem. Soc.* **2017**, *139*, 5720−5723. (b) Escayola, S.; Sola, M.; Poater, A. Mechanism of the Facile Nitrous Oxide Fixation by Homogeneous Ruthenium Hydride Pincer Catalysts. *Inorg. Chem.* **2020**, *59*, 9374−9383. (c) Doyle, L. E.; Piers, W. E.; Borau-Garcia, J. Ligand Cooperation in the Formal Hydrogenation of N_2O Using a PCsp2P Iridium Pincer Complex. *J. Am. Chem. Soc.* **2015**, *137*, 2187−2190.
(26) Zeng, R.; Feller, M.; Diskin-Posner, Y.; Shimon, L. J. W.; Ben-David, Y.; Milstein, D. CO Oxidation by N_2O Homogeneously Catalyzed by Ruthenium Hydride Pincer Complexes Indicating a New Mechanism. *J. Am. Chem. Soc.* **2018**, *140*, 7061−7064.
(27) (a) Rathnayaka, S. C.; Mankad, N. P. Coordination chemistry of the Cuz site in nitrous oxide reductase and its synthetic mimics. *Coord. Chem. Rev.* **2021**, *429*, No. 213718. (b) Bar-Nahum, I.; Gupta, A. K.; Huber, S. M.; Ertem, M. Z.; Cramer, C. J.; Tolman, W. B. Reduction of nitrous oxide to dinitrogen by a mixed valent tricopper-disulfido cluster. *J. Am. Chem. Soc.* **2009**, *131*, 2812−2814. (c) Hsu, C.-W.; Rathnayaka, S. C.; Islam, S. M.; MacMillan, S. N.; Mankad, N. P. N_2O Reductase Activity of a $[Cu_4S]$ Cluster in the 4Cu(I) Redox State Modulated by Hydrogen Bond Donors and Proton Relays in the Secondary Coordination Sphere. *Angew. Chem., Int. Ed.* **2020**, *59*, 627−631. (d) Johnston, E. M.; Dell'Acqua, S.; Pauleta, S. R.; Moura, I.; Solomon, E. I. Protonation state of the Cu_4S_2 CuZ site in nitrous oxide reductase: redox dependence and insight into reactivity. *Chem. Sci.* **2015**, *6*, 5670.
(28) Maitarad, P.; Namuangruk, S.; Zhang, D.; Shi, L.; Li, H.; Huang, L.; Boekfa, B.; Ehara, M. Metal−Porphyrin: A Potential Catalyst for Direct Decomposition of N_2O by Theoretical Reaction Mechanism Investigation. *Environ. Sci. Technol.* **2014**, *48*, 7101−7110.
(29) (a) Becke, A. D. A new mixing of Hartree-Fock and local density-functional theories. *J. Chem. Phys.* **1993**, *98*, 1372−1377. (b) Perdew, J. P.; Ernzerhof, M.; Burke, K. Rationale for mixing exact exchange with density functional approximations. *J. Chem. Phys.* **1996**, *105*, 9982−9985.
(30) Frisch, M. J.; Trucks, G. W.; Schlegel, H. B.; Scuseria, G. E.; Robb, M. A.; Cheeseman, J. R.; Scalmani, G.et al. *Gaussian 09*; Gaussian, Inc.: Wallingford, CT, 2009 (complete citation in SI).
(31) Lu, T. sobMECP Program. http://sobereva.com/286.
(32) Harvey, J. N. Spin-forbidden reactions: computational insight into mechanisms and kinetics. *WIREs Comput. Mol. Sci.* **2014**, *4*, 1−14.
(33) Maeda, S.; Ohno, K.; Morokuma, K. Systematic exploration of the mechanism of chemical reactions: the global reaction route mapping (GRRM) strategy using the ADDF and AFIR methods. *Phys. Chem. Chem. Phys.* **2013**, *15*, 3683−3701.
(34) Legault, C. Y. *CYLview*; CYL Lab, 2019.
(35) (a) Zhang, B.; Sun, L. Ru-bda: Unique Molecular Water-Oxidation Catalysts with Distortion Induced Open Site and Negatively Charged Ligands. *J. Am. Chem. Soc.* **2019**, *141*, 5565−5580. (b) Fukuzumi, S.; Kojima, T.; Lee, Y.-M.; Nam, W. High-valent metal-oxo complexes generated in catalytic oxidation reactions using water as an oxygen source. *Coord. Chem. Rev.* **2017**, *333*, 44−56. (c) Zeng, Q.; Lewis, F. W.; Harwood, L. M.; Hartl, F. Role of ligands in catalytic water oxidation by mononuclear ruthenium complexes. *Coord. Chem. Rev.* **2015**, *304*−*305*, 88−101. (d) Matheu, R.; Garrido-Barros, P.; Gil-Sepulcre, M.; Ertem, M. Z.; Sala, X.; Gimbert-Suriñach, C.; Llobet, A. The Development of Molecular Water Oxidation Catalysts. *Nat. Rev. Chem.* **2019**, *3*, 331−341.
(36) (a) Duan, L.; Bozoglian, F.; Mandal, S.; Stewart, B.; Privalov, T.; Llobet, A.; Sun, L. A molecular ruthenium catalyst with water-oxidation activity comparable to that of photosystem II. *Nat. Chem.* **2012**, *4*, 418. (b) Richmond, C. J.; Matheu, R.; Poater, A.; Falivene, L.; Benet-Buchholz, J.; Sala, X.; Cavallo, L.; Llobet, A. Supramolecular Water Oxidation with Ru-bda-Based Catalysts. *Chem.—Eur. J.* **2014**, *20*, 17282. (c) Luque-Urrutia, J. A.; Solà, M.; Poater, A. The influence of the pH on the reaction mechanism of water oxidation by a Ru(bda) catalyst. *Catal. Today* **2020**, *358*, 278. (d) Kang, R.; Chen, K.; Yao, J.; Shaik, S.; Chen, H. Probing Ligand Effects on O-O Bond Formation of Ru-Catalyzed Water Oxidation: A Computational Survey. *Inorg. Chem.* **2014**, *53*, 7130−7136.
(37) (a) Zuberbühler, A. D. Dicopper and heteronuclear iron-copper peroxo complex formation: kinetics and thermodynamics. *Micron* **2004**, *35*, 133−135. (b) Bossek, U.; Weyhermueller, T.; Wieghardt, K.; Nuber, B.; Weiss, J. $[L_2Mn_2(\mu\text{-}O)_2(\mu\text{-}O_2)](ClO_4)_2$. The first binuclear ($\mu$-peroxo) dimanganese(IV) complex (L = 1, 4, 7-trimethyl-1, 4, 7- triazacyclononane). A model for the S4 → S0 transformation in the oxygen- evolving complex in photosynthesis. *J. Am. Chem. Soc.* **1990**, *112*, 6387−6388.
(38) (a) Gubelmann, M. H.; Williams, A. F. The Structure and Reactivity of Dioxygen Complexes of the Transition Metals. In *Transition Metal Complexes-Structure and Spectra*; Springer, 1983; Vol. 55, pp 1−65. (b) Wagnerová, D. M.; Lang, K. Photorelease of triplet and singlet oxygen from dioxygen complexes. *Coord. Chem. Rev.* **2011**, *255*, 2904−2911.
(39) (a) Itoh, S. Developing Mononuclear Copper-Active-Oxygen Complexes Relevant to Reactive Intermediates of Biological Oxidation Reactions. *Acc. Chem. Res.* **2015**, *48*, 2066−2074. (b) Bertini, L.; Breglia, R.; Lambrughi, M.; Fantucci, P.; De Gioia, L.; Borsari, M.; Sola, M.; Bortolotti, C. A.; Bruschi, M. Catalytic Mechanism of Fungal Lytic Polysaccharide Monooxygenases Investigated by First-Principles Calculations. *Inorg. Chem.* **2018**, *57*, 86−97. (c) Vilella, L.; Conde, A.; Balcells, D.; Diaz-Requejo, M. M.; Lledos, A.; Perez, P. J. A competing, dual mechanism for catalytic direct benzene hydroxylation from combined experimental-DFT studies. *Chem. Sci.* **2017**, *8*, 8373−8383.
(40) (a) Hatcher, L. Q.; Karlin, K. D. Ligand Influences in Copper-Dioxygen Complex-Formation and Substrate Oxidations. In *Advances in Inorganic Chemistry*, Elsevier Inc., 2006; Vol. 58, pp 131−184. (b) Mirica, L. M.; Ottenwaelder, X.; Stack, T. D. P. Structure and Spectroscopy of Copper-Dioxygen Complexes. *Chem. Rev.* **2004**, *104*, 1013−1045.
(41) (a) Coates, C. J.; Costa-Paiva, E. M. Multifunctional Roles of Hemocyanins. In *Vertebrate and Invertebrate Respiratory Proteins, Lipoproteins and other Body Fluid Proteins*, Subcellular Biochemistry; Springer, pp 233−250. (b) Peterson, R. L.; Kim, S.; Karlin, K. D. Copper Enzymes. In *Comprehensive Inorganic Chemistry II*; Reedijk, J.; Poeppelmeier, K., Eds.; Elsevier, 2013; Vol. 3, pp 149−177. (c) Rebilly, J.-N.; Reinaud, O. Supramolecular Copper Dioxygen Chemistry. *Copper−Oxygen Chemistry*; Wiley Series on Reactive Intermediates in Chemistry and Biology; John Wiley & Sons, Inc., pp 321−360. (d) Saito, T.; Thiel, W. Quantum Mechanics/Molecular Mechanics Study of Oxygen Binding in Hemocyanin. *J. Phys. Chem. B* **2014**, *118*, 5034−5043.
(42) (a) Hinokuma, S.; Iwasa, T.; Kon, Y.; Taketsugu, T.; Sato, K. N_2O decomposition properties of Ru catalysts supported on various oxide materials and SnO_2. *Sci. Rep.* **2020**, *10*, No. 21605. (b) Chang, Y.-F.; McCarty, J. G.; Wachsman, E. D. Effect of ruthenium-loading on the catalytic activity of Ru-NaZSM-5 zeolites for nitrous oxide decomposition. *Appl. Catal., B* **1995**, *6*, 21−33. (c) Li, Y.; Armor, J. N. Catalytic decomposition of nitrous oxide on metal exchanged zeolites. *Appl. Catal., B* **1992**, *1*, L21−29.
(43) (a) Duan, L.; Bozoglian, F.; Mandal, S.; Stewart, B.; Privalov, T.; Llobet, A.; Sun, L. A Molecular Ruthenium Catalyst with Water-Oxidation Activity Comparable to That of Photosystem II. *Nat. Chem.* **2012**, *4*, 418−423. (b) Xie, Y.; Shaffer, D. W.; Concepcion, J. J. O-O Radical Coupling: From Detailed Mechanistic Understanding to

Enhanced Water Oxidation Catalysis. *Inorg. Chem.* **2018**, *57*, 10533−10542.

(44) (a) Zhou, X.-T.; Ji, H. B.; Cheng, Z.; Xu, J.-C.; Pei, L.-X.; Wang, L.-F. Selective oxidation of sulfides to sulfoxides catalyzed by ruthenium(III) *meso*-tetraphenylporphyrin chloride in the presence of molecular oxygen. *Bioorg. Med. Chem. Lett.* **2007**, *17*, 4650−4653. (b) Zhou, X.-T.; Ji, H.-B.; Yuan, Q.-L. Baeyer-Villiger oxidation of ketones catalyzed by iron(III) meso-tetraphenylporphyrin chloride in the presence of molecular oxygen. *J. Porphyrins Phthalocyanines* **2008**, *12*, 94−100.

(45) (a) Zhang, R.; Vanover, E.; Luo, W.; Newcomb, M. Photochemical generation and kinetic studies of a putative porphyrin-ruthenium(V)-oxo species. *Dalton Trans.* **2014**, *43*, 8749−8756. (b) Shing, K.-P.; Cao, B.; Liu, Y.; Lee, H. K.; Li, M.-D.; Phillips, D. L.; Chang, X.-Y.; Che, C.-M. Arylruthenium(III) Porphyrin-Catalyzed C-H Oxidation and Epoxidation at Room Temperature and [Ru(V)(Por)(O)(Ph)] Intermediate by Spectroscopic Analysis and Density Functional Theory Calculations. *J. Am. Chem. Soc.* **2018**, *140*, 7032−7042.

(46) (a) Mori, T.; Yamaguchi, M.; Yamagishi, T. Hydrogen peroxide oxidation of olefin catalyzed by polyaminopolycarboxylatoruthenium(III) complexes. *Nippon Kagaku Kaishi* **1997**, *5*, 329−334. (b) Kratz, F.; Messori, L. Spectral characterization of ruthenium(III) transferrin. *J. Inorg. Biochem.* **1993**, *49*, 79−82.

(47) Teffo, J.-L.; Chedin, A. Internuclear Potential and Equilibrium Structure of the Nitrous Oxide Molecule from Rovibrational Data. *J. Mol. Spectrosc.* **1989**, *135*, 389−409.

(48) (a) A scaling factor of 0.94, derived from the ratio of DFT-calculated/experimental frequencies for N_2O, was applied to the calculated vibrational frequencies of LM-N_2O to compare with experimental data. (b) Rauhut, G.; Pulay, P. Transferable Scaling Factors for Density Functional Derived Vibrational Force Fields. *J. Phys. Chem. A* **1995**, *99*, 3093−3100.

(49) Cotton, F. A.; Wilkinson, G.; Murillo, C. A.; Bochmann, M. *Advanced Inorganic Chemistry*, 6th ed.; Wiley, 1999; pp 856−858.

(50) (a) Kryachko, E. S.; Vinckier, C.; Nguyen, M. T. Another look at the electron attachment to nitrous oxide. *J. Chem. Phys.* **2001**, *114*, 7911−7917. (b) Takahashi, K.; Ohgami, S.; Koyama, Y.; Sawamura, S. D.; Marin, T. W.; Bartels, D. M.; Jonah, C. D. Reaction rates of the hydrated electron with N_2O in high temperature water and potential surface of the N_2O^- anion. *Chem. Phys. Lett.* **2004**, *383*, 445−450.

(51) Andino, J. G.; Caulton, K. G. Mechanism of N/O Bond Scission of N_2O by an Unsaturated Rhodium Transient. *J. Am. Chem. Soc.* **2011**, *133*, 12576−12583.

(52) Magnus, K. A.; Hazes, B.; Ton-That, H.; Bonaventura, C.; Bonaventura, J.; Hol, W. G. Crystallographic analysis of oxygenated and deoxygenated states of arthropod hemocyanin shows unusual differences. *Proteins* **1994**, *19*, 302−309.

(53) Aboelella, N. W.; Lewis, E. A.; Reynolds, A. M.; Brennessel, W. W.; Cramer, C. J.; Tolman, W. B. Snapshots of Dioxygen Activation by Copper: The Structure of a 1:1 Cu/O_2 Adduct and Its Use in Syntheses of Asymmetric Bis(μ-oxo) Complexes. *J. Am. Chem. Soc.* **2002**, *124*, 10660−10661.

(54) Tachi, Y.; Aita, K.; Teramae, S.; Fumito, T.; Naruta, Y.; Fukuzumi, S.; Itoh, S. Dicopper-Dioxygen Complex Supported by Asymmetric Pentapyridine Dinucleating Ligand. *Inorg. Chem.* **2004**, *43*, 4558−4560.

(55) (a) Husch, T.; Freitag, L.; Reiher, M. Calculation of Ligand Dissociation Energies in Large Transition-Metal Complexes. *J. Chem. Theory Comput.* **2018**, *14*, 2456−2468. (b) Bao, J. L.; Welch, B. K.; Ulusoy, I. S.; Zhang, X.; Xu, X.; Wilson, A. K.; Truhlar, D. G. Predicting Bond Dissociation Energies and Bond Lengths of Coordinatively Unsaturated Vanadium-Ligand Bonds. *J. Phys. Chem. A* **2020**, *124*, 9757−9770. (c) Lakuntza, O.; Besora, M.; Maseras, F. Searching for Hidden Descriptors in the Metal-Ligand Bond through Statistical Analysis of Density Functional Theory (DFT) Results. *Inorg. Chem.* **2018**, *57*, 14660−14670. (d) Chen, M.; Craciun, R.; Hoffman, N.; Dixon, D. A. Ligand Bond Energies in cis- and *trans*-[L-Pd$(PH_3)_2$Cl]$^+$ Complexes from Coupled Cluster Theory (CCSDT) and Density Functional Theory. *Inorg. Chem.* **2012**, *51*, 13195−13203.

(56) (a) Costa, J. I. T.; Tome, A. C.; Neves, M. G. P. M. S.; Cavaleiro, J. A. S. 10, 15, 20-tetrakis(pentafluorophenyl) porphyrin: a versatile platform to novel porphyrinic materials. *J. Porphyrins Phthalocyanines* **2011**, *15*, 1116−1133. (b) Vinhado, F. S.; Martins, P. R.; Iamamoto, Y. Metalloporphyrins as efficient models of heme-enzymes in oxidation reactions. *Curr. Top. Catal.* **2002**, *3*, 199−213. (c) Alexiou, C.; Lever, A. B. P. Tuning metalloporphyrin and metallophthalocyanine redox potentials using ligand electrochemical (EL) and Hammett (σ,ρ) parametrization. *Coord. Chem. Rev.* **2001**, *216−217*, 45−54.

(57) Swann, M. T.; Nicholas, K. M. Structural Effects on Dioxygen Evolution from Ru(V)-Oxo Complexes. *Eur. J. Inorg. Chem.* **2021**, *2021*, 3565−3577.

(58) Khan, M. M. T.; Mizra, S. A.; Shaikh, Z. A.; Sreelatha, C.; Paul, P.; Shukla, R. S.; Srinivas, D.; Rao, A. P.; Abdi, S. H. R.; Bhatt, S. D.; Ramachandraiah, G. Dioxygen Affinities of Some Ruthenium(III) Schiff Base Complexes. *Polyhedron* **1992**, *11*, 1821−1827.

(59) (a) Collman, J. P.; Fish, H. T. A Bis-Capped Cofacial Metallodiporphyrin: Synthesis and Electrochemistry of a Molecule Containing Two Coaxial Metal-Metal Multiple Bonds in Close Proximity. *Inorg. Chem.* **1996**, *35*, 7922−7923. (b) Isobe, H.; Tanaka, K.; Shen, J.-R.; Yamaguchi, K. Water Oxidation Chemistry of a Synthetic Dinuclear Ruthenium Complex Containing Redox-Active Quinone Ligands. *Inorg. Chem.* **2014**, *53*, 3973−3984. (c) Sander, A. C.; Maji, S.; Franc, L.; Bçhnisch, T.; Dechert, S.; Llobet, A.; Meyer, F. Highly Efficient Binuclear Ruthenium Catalyst for Water Oxidation. *ChemSusChem* **2015**, *8*, 1697−1702. (d) Guilard, R.; Lopez, M. A.; Tabard, A.; Richard, P.; Lecomte, C.; Brandes, S.; Hutchison, J. E.; Collman, J. P. Synthesis and characterization of novel cobalt aluminum cofacial porphyrins. First crystal and molecular structure of a heterobimetallic biphenylene pillared cofacial diporphyrin. *J. Am. Chem. Soc.* **1992**, *114*, 9877−9889.

https://doi.org/10.1021/acs.inorgchem.2c01598
Inorg. Chem. 2022, 61, 14591−14605